

Neutrino Masses at LHC: Minimal Lepton Flavour Violation in Type-III See-saw

O. J. P. Éboli

Instituto de Física, Universidade de São Paulo, São Paulo – SP, Brazil.
E-mail: eboli@fma.if.usp.br

J. Gonzalez-Fraile

Departament d'Estructura i Constituents de la Matèria and ICC-UB, Universitat de Barcelona, 647 Diagonal, E-08028 Barcelona, Spain
E-mail: fraile@ecm.ub.es

M. C. Gonzalez-Garcia

Institució Catalana de Recerca i Estudis Avançats (ICREA), Departament d'Estructura i Constituents de la Matèria, Universitat de Barcelona, 647 Diagonal, E-08028 Barcelona, Spain
and: *C.N. Yang Institute for Theoretical Physics, SUNY at Stony Brook, Stony Brook, NY 11794-3840, USA*
E-mail: concha@insti.physics.sunysb.edu

ABSTRACT: We study the signatures of minimal lepton flavour violation in a simple Type-III see-saw model in which the flavour scale is given by the new fermion triplet mass and it can be naturally light enough to be produced at the LHC. In this model the flavour structure of the lepton number conserving couplings of the triplet fermions to the Standard Model leptons can be reconstructed from the neutrino mass matrix and the smallness of the neutrino mass is associated with a tiny violation of total lepton number. Characteristic signatures of this model include suppressed lepton number violation decays of the triplet fermions, absence of displaced vertices in their decays and predictable lepton flavour composition of the states produced in their decays. We study the observability of these signals in the processes $pp \rightarrow 3\ell + 2j + \cancel{E}_T$ and $pp \rightarrow 2\ell + 4j$ with $\ell = e$ or μ taking into account the present low energy data on neutrino physics and the corresponding Standard Model backgrounds. Our results indicate that the new fermionic states can be observed for masses up to 500 GeV depending on the CP violating Majorana phase for an integrated luminosity of 30 fb^{-1} . Moreover, the flavour of the final state leptons in the above processes can shed light on the neutrino mass ordering.

Contents

1. Introduction	1
2. Simplest MLFV Type-III see-saw model	3
3. Signatures	9
4. Process $pp \rightarrow \ell\ell jj\cancel{E}_T$	12
5. Process $pp \rightarrow \ell\ell jjjj$	20
6. Signals at 7 TeV	25
7. Summary and discussions	27

1. Introduction

The observation of neutrino masses and mixing is our first evidence of physics beyond the Standard Model (SM) [1]. The CERN Large Hadron Collider (LHC) has started operation with the aim of exploring physics beyond SM at the TeV scale. Then, an obviously interesting question is whether the new physics (NP) associated to the neutrino masses can be within the LHC reach. Here we analyze the LHC potential to unravel the existence of triplet fermionic states that appear in minimal flavour violating theories based on Type-III see-saw models of neutrino mass. We also discuss how to probe the neutrino mass ordering in the production and decay of these new possible states.

NP effects at energies below the characteristic NP scale can be described in terms of effective higher-dimension ($d > 4$) operators and it is well known that, with the particle contents of the SM, there is just one dimension-five operator which can be built [2], $\alpha_5/\Lambda_{\text{LN}}\mathcal{O}_5 = \alpha_5/\Lambda_{\text{LN}}L_L L_L H H$, where L_L and H are the leptonic and Higgs $SU(2)_L$ doublets. This operator breaks total lepton number and after electroweak symmetry breaking it generates Majorana masses for the neutrinos $m_\nu \sim \alpha_5 v^2/\Lambda_{\text{LN}}$, where v is the SM Higgs vacuum expectation value (vev). Consequently neutrinos are much lighter than the other SM fermions because of the large scale of total lepton number violation Λ_{LN} . In simple renormalizable realizations of NP this dimension-5 operator can be generated by the tree-level exchange of three types of new particles:

- Type-I see-saw [3]: One adds at least two fermionic singlets of mass M and the neutrino masses are $m_\nu \sim \lambda^2 v^2/M$, where λ is the Yukawa coupling.

- Type-II see-saw [4]: One adds an $SU(2)_L$ Higgs triplet Δ of mass M and with a neutral component which in presence of scalar doublet-triplet mixing μ term in the scalar potential acquires a vev $v_\Delta = \mu v^2/M^2$. The neutrino masses are $m_\nu \sim \lambda \mu v^2/M^2$.
- Type-III see-saw [5]: One adds at least two $SU(2)_L$ fermion triplets with zero hypercharge generating neutrino masses, $m_\nu \sim \lambda^2 v^2/M$.

In addition hybrid scenarios containing some combination of these states have also been constructed [6]. In any of these mechanisms the smallness of the neutrino mass can be naturally explained with Yukawa couplings $\lambda \sim \mathcal{O}(1)$ if the masses of the heavy states are $M \sim \Lambda_{LN} \sim 10^{14-15}$ GeV (with $\mu \sim M$ also for Type-II), clearly out of reach of the LHC.

Since strictly nothing prevents that the new states have TeV scale masses, there has been an increasing literature studying the possible signatures of these neutrino-mass-inducing states with TeV-scale masses at the LHC (see e.g. [7–12]). Nevertheless, in some cases such a low-scale M is technically unnatural or, in some others, it is simply not very well motivated theoretically. Notwithstanding consistent models of TeV-scale see-saw exist in the literature for some time (see e.g. [13, 14]).

Generically, at low energies the Lagrangian of the full theory can be expanded as

$$\mathcal{L} = \mathcal{L}_{SM} + \frac{\alpha_5}{\Lambda_{LN}} \mathcal{O}_5 + \sum_i \frac{\alpha_{6,i}}{\Lambda_{FL}^2} \mathcal{O}_{6,i} + \dots \quad (1.1)$$

where \mathcal{O}_5 is Weinberg’s operator responsible for neutrino masses, and $\mathcal{O}_{6,i}$ are flavour-changing, but lepton number conserving, dimension-6 operators. In this context attractive TeV-scale see-saw models are those for which it is possible to relate the mass of the new states $M \sim \Lambda_{FL} \sim \mathcal{O}(\text{TeV})$ but still keep $\Lambda_{LN} \gg \Lambda_{FL}$ to explain the smallness of the neutrino mass. This is different than the simplest implementations described above for which $M \sim \Lambda_{LN} \sim \Lambda_{FL}$.

In this effective operator approach the possibility of TeV scale see-saw models has been recently revised in the context of minimal lepton flavour violation (MLFV) [15–18]. Minimal flavour violation was first introduced for quarks [19] as a way to explain the absence of NP effects in flavour changing processes in meson decays. The basic assumption is that the only source of flavour mixing in the full theory is the same as in the SM, *i.e.* the quark Yukawa couplings. This idea was latter on extended for leptons [16, 17] although for leptons the precise hypothesis corresponding to MLFV is less well-defined as the SM only contains Yukawa couplings for the charged leptons and those are not enough to explain the neutrino data. Consequently, the couplings and generation structure of the new states must also be considered when defining the conditions for MLFV, making them model dependent by default.

In Ref. [15] simple see-saw models were constructed which realize the conditions associated with MLFV as set-up in Ref. [16], *i.e.* there is large hierarchy between the lepton number and lepton flavour breaking scales, $\Lambda_{LN} \gg \Lambda_{FL}$, and the coefficients $\alpha_{6,i}$ are determined by α_5 . As discussed in Ref. [15] these conditions are automatically fulfilled by the simplest Type-II see-saw model if a light double-triplet mixing μ is assumed. For LHC

phenomenology this leads to the interesting possibility studied in detail in Refs. [9, 20] of the production of the triplet scalar states with all their decay modes determined by the neutrino mass parameters. From the theoretical side, one drawback of such a scenario is that it is difficult to keep such a low μ stable if generated by spontaneous breaking of lepton number. In the same work [15] the authors presented a very simple model for Type-I or Type-III see-saw with naturally light states. From the point of view of LHC phenomenology these models are attractive since, a) the new states can be light enough to be produced at LHC, and b) their observable (ie the lepton number conserving) signatures are fully determined by the neutrino parameters. In Type-I see-saw the new states are SM singlets, and therefore, they can only be produced via their mixing with the SM neutrinos. This leads to small production rates which makes the model only marginally testable at LHC. Type-III see-saw fermions, on the contrary, are SM triplets with weak-interaction pair-production cross section, and consequently, having the potential to allow for tests of the hypothesis of MLFV. This is the scenario which we explore in this work. Alternatively, signals of MLFV in a model in which the MLFV condition does not involve the states associated with the generation of neutrino mass has been explored in Ref. [21].

The outline of this work is as follows. In Sec. 2 we summarize the basics of the model in which the flavour scale is given by the new fermion triplet mass and it can be naturally light to be within reach at LHC. We describe how in this model the flavour structure of the lepton number conserving couplings of the triplet fermions, and consequently their observable decay branching ratios to the SM leptons, can be reconstructed from the neutrino mass matrix. In this model the lightness of the neutrino mass implies that lepton number violating decay modes of the triplet fermions are suppressed. Section 3 describes the generic features of the expected total lepton number conserving signatures. In Sec. 4 we evaluate in detail the signal and backgrounds for the process $pp \rightarrow \ell\ell jj \cancel{E}_T$ for which the challenge is the identification/assignment of the lepton corresponding to the decay chain of each of the fermion triplets. Section 5 contains our analysis of the discovery potential of the process $pp \rightarrow \ell\ell jjjj$ which presents a larger QCD background. For both final states we evaluate the expected signals within the presently allowed ranges of neutrino parameters, we study their statistical significance as a function of those for fermion triplet masses in the range 150–500 GeV and we also discuss how to probe the neutrino mass ordering in these final states. These studies are done for the LHC running at 14 TeV. We comment on Sec. 6 the potential of the 7 TeV run. Finally we summarize our conclusions in Sec. 7.

2. Simplest MLFV Type-III see-saw model

We describe here the simplest MLFV model presented in Ref. [15] adapted for Type-III see-saw. As explained above, Type-I see-saw heavy fermions are SM singlets, and therefore, they can only be produced via their mixing with the SM neutrinos. This leads to small production rates which makes the model only marginally testable at LHC.

In this MLFV Type-III see-saw model the SM Lagrangian is extended with two fermion triplets $\vec{\Sigma} = (\Sigma_1, \Sigma_2, \Sigma_3)$ and $\vec{\Sigma}' = (\Sigma'_1, \Sigma'_2, \Sigma'_3)$, each one formed by three right-handed

Weyl spinors of zero hypercharge. Hence, the Lagrangian is

$$\mathcal{L} = \mathcal{L}_{SM} + \mathcal{L}_K + \mathcal{L}_Y + \mathcal{L}_\Lambda \quad (2.1)$$

with

$$\mathcal{L}_K = i \left(\bar{\vec{\Sigma}} \not{D}_\mu \vec{\Sigma} + \bar{\vec{\Sigma}'} \not{D}_\mu \vec{\Sigma}' \right) \quad (2.2)$$

$$\mathcal{L}_Y = -Y_i^\dagger \bar{L}_{Li}^w \left(\vec{\Sigma} \cdot \vec{\tau} \right) \tilde{\phi} - \epsilon Y_i'^\dagger \bar{L}_{Li}^w \left(\vec{\Sigma}' \cdot \vec{\tau} \right) \tilde{\phi} + h.c. \quad (2.3)$$

$$\mathcal{L}_\Lambda = -\frac{\Lambda}{2} \left(\bar{\vec{\Sigma}}^c \vec{\Sigma}' + \bar{\vec{\Sigma}'}^c \vec{\Sigma} \right) - \frac{\mu}{2} \bar{\vec{\Sigma}'}^c \vec{\Sigma}' - \frac{\mu'}{2} \bar{\vec{\Sigma}}^c \vec{\Sigma} + h.c. \quad (2.4)$$

Here $\vec{\tau}$ are the Pauli matrices, the gauge covariant derivative is given by $D_\mu = \partial_\mu + ig \vec{T} \cdot \vec{W}_\mu$, where \vec{T} are the three-dimensional representation of the $SU(2)$ generators, ϕ is the SM Higgs doublet, and $L_i^w = (\nu_i^w, \ell_i^w)^T$ are the three lepton doublets of the SM. The index w makes reference at the fact that these are weak-eigenstates to be distinguish from those without the index which will be the mass eigenstates.

In the MLFV Type-III see-saw model the flavour-blind parameters ϵ , μ and μ' are *small*, ie, the scales μ and μ' are much smaller than Λ and v and $\epsilon \ll 1$. As a consequence the Lagrangian in Eq. (2.1) breaks total lepton number due to the simultaneous presence of the Yukawa terms Y_i and $\epsilon Y_i'$ as well as to the presence of the μ and μ' terms. In the limit $\mu, \mu', \epsilon \rightarrow 0$ it is possible to define a conserved total lepton number by assigning $L(L^w) = L(\Sigma) = -L(\Sigma') = 1$.

After electroweak symmetry breaking and working in the unitary gauge, $\tilde{\phi}^T = \frac{1}{\sqrt{2}} (v \ 0)$, the six Weyl fermions of well defined electric charge are $\Sigma_\pm^{(\prime)} = \frac{1}{\sqrt{2}} \left(\Sigma_1^{(\prime)} \mp i \Sigma_2^{(\prime)} \right)$ and $\Sigma_0^{(\prime)} = \Sigma_3^{(\prime)}$. From those one defines the negatively charged Dirac fermions E and E' and the neutral Majorana fermions \tilde{N} and \tilde{N}'

$$E^{(\prime)} = \Sigma_-^{(\prime)} + \Sigma_+^{(\prime)c} \quad \tilde{N}^{(\prime)} = \Sigma_0^{(\prime)} + \Sigma_0^{(\prime)c}. \quad (2.5)$$

In this basis the leptonic mass terms read

$$\mathcal{L}_m = -\frac{1}{2} \left(\bar{\nu}_L^w \bar{\tilde{N}}_R \bar{\tilde{N}}_R' \right) M_0 \begin{pmatrix} \nu_L^w \\ \tilde{N}_R^c \\ \tilde{N}_R'^c \end{pmatrix} - \left(\bar{\ell}_L^w \bar{E}_L \bar{E}_L' \right) M_\pm \begin{pmatrix} \ell_R^w \\ E_R \\ E_R' \end{pmatrix} + h.c \quad (2.6)$$

with

$$M_0 = \begin{pmatrix} 0 & \frac{v}{\sqrt{2}} Y^T & \epsilon \frac{v}{\sqrt{2}} Y'^T \\ \frac{v}{\sqrt{2}} Y & \mu' & \Lambda \\ \epsilon \frac{v}{\sqrt{2}} Y' & \Lambda & \mu \end{pmatrix} \quad M_\pm = \begin{pmatrix} \frac{v}{\sqrt{2}} Y^\ell & v Y^\dagger & \epsilon v Y'^\dagger \\ 0 & \mu' & \Lambda \\ 0 & \Lambda & \mu \end{pmatrix} \quad (2.7)$$

where Y^ℓ are the charged lepton Yukawa couplings of the SM and $Y^{(\prime)} = (Y_1^{(\prime)}, Y_2^{(\prime)}, Y_3^{(\prime)})$. In writing Eq. (2.6) we denote by $\vec{\nu}^w$ and $\vec{\ell}^w$ two column vectors containing the three neutrinos and charged leptons of the SM in the weak basis respectively. Furthermore,

without loss of generality, we have chosen to work in a basis in which Λ is real while both Y and Y' are complex. In general the parameters μ and μ' would be complex, but for the sake of simplicity we have taken them to be real in what follows though it is straight forward to generalize the expression to include the relevant phases [24].

Diagonalizing \mathcal{L}_m one finds three light Majorana neutrinos ν_i – the lightest being massless – and three light charged massive leptons ℓ_i that satisfy

$$m_\nu^{diag} = V^{\nu T} \left[-\frac{v^2}{2\Lambda} \epsilon \left(\widehat{Y'}^T Y + Y^T \widehat{Y'} \right) \right] V^\nu, \quad (2.8)$$

$$m_\ell^{diag} = \frac{v}{\sqrt{2}} V_R^{\ell \dagger} Y^{\ell \dagger} \left[1 - \frac{v^2}{2\Lambda^2} Y^\dagger Y \right] V_L^\ell. \quad (2.9)$$

V^ν and $V_{L,R}^\ell$ being 3×3 unitary matrices and for convenience we have defined the combination

$$\widehat{Y'} = Y' - \frac{1}{\epsilon} \frac{\mu}{2\Lambda} Y. \quad (2.10)$$

One finds also two heavy Majorana neutral leptons and two charged heavy leptons with masses $M \simeq \Lambda(1 \mp \frac{\mu \pm \mu'}{2\Lambda})$. We construct a quasi-Dirac state N with the two Majorana neutral leptons and two combinations of the heavy charged leptons E_1^- and E_2^+ which are related to the weak eigenstates by

$$\nu_L^w = V^\nu \nu_L + \frac{v}{\sqrt{2}\Lambda} Y^\dagger N_L + \frac{v}{\sqrt{2}\Lambda} \left(\epsilon Y'^\dagger - \left(\frac{3\mu + \mu'}{4\Lambda} \right) Y^\dagger \right) N_R^c, \quad (2.11)$$

$$\ell_L^w = \ell_L + \frac{v}{\Lambda} Y^\dagger E_{1L}^- + \frac{v}{\Lambda} \left(\epsilon Y'^\dagger - \left(\frac{3\mu + \mu'}{4\Lambda} \right) Y^\dagger \right) E_{2R}^{+c}, \quad (2.12)$$

$$\ell_R^w = \ell_R, \quad (2.13)$$

$$N_L = N_R^c - \left(\frac{\mu - \mu'}{4\Lambda} \right) N_L - \frac{v}{\sqrt{2}\Lambda} \left(\epsilon Y' - \frac{\mu}{\Lambda} Y \right) V^\nu \nu_L, \quad (2.14)$$

$$N_L' = N_L + \left(\frac{\mu - \mu'}{4\Lambda} \right) N_R^c - \frac{v}{\sqrt{2}\Lambda} Y V^\nu \nu_L, \quad (2.15)$$

$$E_L = E_{2R}^{+c} - \left(\frac{\mu - \mu'}{4\Lambda} \right) E_{1L}^- - \frac{v}{\Lambda} \left(\epsilon Y' - \frac{\mu}{\Lambda} Y \right) \ell_L, \quad (2.16)$$

$$E_R = E_{1R}^- - \left(\frac{\mu - \mu'}{4\Lambda} \right) E_{2L}^{+c}, \quad (2.17)$$

$$E_L' = E_{1L}^- + \left(\frac{\mu - \mu'}{4\Lambda} \right) E_{2R}^{+c} - \frac{v}{\Lambda} Y \ell_L, \quad (2.18)$$

$$E_R' = E_{2L}^{+c} + \left(\frac{\mu - \mu'}{4\Lambda} \right) E_{1R}^-. \quad (2.19)$$

where we have used that, in general, one can choose the flavour basis such as $V_L^\ell = V_R^\ell = I$.

To first order in the small parameters the neutral weak interactions of the light states take the same form as that on the SM and the charged current interactions read ¹

$$\mathcal{L}_W^{light} = -\frac{g}{\sqrt{2}} (\overline{\ell}_L \gamma^\mu U_{LEP} \nu_L W_\mu^-) + h.c. \quad (2.20)$$

¹Violation of unitarity (and flavour mixing) appears in the CC (and NC) interactions of the light leptons to higher order [22–24].

where g is the $SU(2)_L$ coupling constant.

After absorbing three unphysical phases in the definition of the light charged leptons, the leptonic mixing matrix can be chosen

$$U_{LEP} = V^\nu = \begin{pmatrix} 1 & 0 & 0 \\ 0 & c_{23} & s_{23} \\ 0 & -s_{23} & c_{23} \end{pmatrix} \begin{pmatrix} c_{13} & 0 & s_{13}e^{-i\delta_{CP}} \\ 0 & 1 & 0 \\ -s_{13}e^{i\delta_{CP}} & 0 & c_{13} \end{pmatrix} \begin{pmatrix} c_{21} & s_{12} & 0 \\ -s_{12} & c_{12} & 0 \\ 0 & 0 & 1 \end{pmatrix} \begin{pmatrix} e^{-i\alpha} & 0 & 0 \\ 0 & e^{i\alpha} & 0 \\ 0 & 0 & 1 \end{pmatrix}, \quad (2.21)$$

where $c_{ij} \equiv \cos \theta_{ij}$ and $s_{ij} \equiv \sin \theta_{ij}$. The angles θ_{ij} can be taken without loss of generality to lie in the first quadrant, $\theta_{ij} \in [0, \pi/2]$ and the phases δ_{CP} , $\alpha \in [0, 2\pi]$. The leptonic mixing matrix contains only two phases because there are only two heavy triplets and consequently only two light neutrinos are massive while the lightest one remains massless.

As shown in Ref. [15] in this simple model one can fully reconstruct the neutrino Yukawa coupling Y and the combination \widehat{Y}' from the neutrino mass matrix. Therefore it is not possible to reconstruct the Yukawa couplings Y' from Eq. (2.10) without the knowledge of the parameters ϵ and μ . The reconstruction is different for normal and inverted orderings:

- Normal Ordering (NO): In this case we have $0 = m_1 < m_2 < m_3$ and the Yukawa couplings are given by

$$Y_a = \frac{y}{\sqrt{2}} \left(\sqrt{1+\rho} U_{a3}^* + \sqrt{1-\rho} U_{a2}^* \right), \quad (2.22)$$

$$\widehat{Y}'_a = \frac{\widehat{y}'}{\sqrt{2}} \left(\sqrt{1+\rho} U_{a3}^* - \sqrt{1-\rho} U_{a2}^* \right),$$

where y and \widehat{y}' are two real numbers and

$$\rho = \frac{\sqrt{1+r} - \sqrt{r}}{\sqrt{1+r} + \sqrt{r}}, \quad r = \frac{m_2^2 - m_1^2}{m_3^2 - m_2^2}, \quad (2.23)$$

$$m_1 = 0, \quad m_2 = \frac{\epsilon y \widehat{y}' v^2}{\Lambda} (1 - \rho), \quad m_3 = \frac{\epsilon y \widehat{y}' v^2}{\Lambda} (1 + \rho). \quad (2.24)$$

- Inverted Ordering (IO): If we have $0 = m_3 < m_1 < m_2$ the Yukawa can be written as

$$Y_a = \frac{y}{\sqrt{2}} \left(\sqrt{1+\rho} U_{a2}^* + \sqrt{1-\rho} U_{a1}^* \right), \quad (2.25)$$

$$\widehat{Y}'_a = \frac{\widehat{y}'}{\sqrt{2}} \left(\sqrt{1+\rho} U_{a2}^* - \sqrt{1-\rho} U_{a1}^* \right),$$

with

$$\rho = \frac{\sqrt{1+r} - 1}{\sqrt{1+r} + 1}, \quad r = \frac{m_2^2 - m_1^2}{m_1^2 - m_3^2}, \quad (2.26)$$

$$m_3 = 0, \quad m_1 = \frac{\epsilon y \widehat{y}' v^2}{\Lambda} (1 - \rho), \quad m_2 = \frac{\epsilon y \widehat{y}' v^2}{\Lambda} (1 + \rho). \quad (2.27)$$

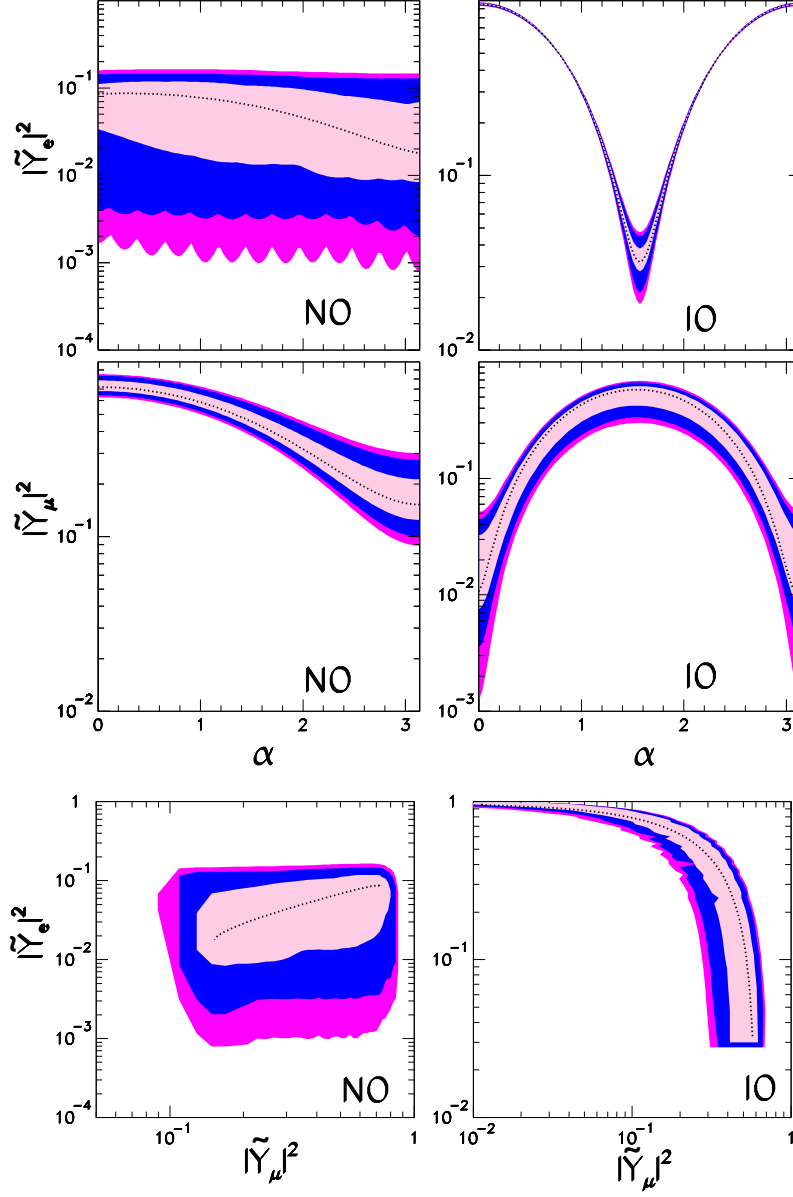


Figure 1: Allowed ranges of the Yukawa couplings $|\tilde{Y}_e|^2 \equiv |Y_1|^2/y^2$ and $|\tilde{Y}_\mu|^2 \equiv |Y_2|^2/y^2$ obtained from the global analysis of neutrino data [25]. The upper four panel shows the values of the couplings as a function of the unknown Majorana phase α . The correlation between the two couplings is own in the two lower panels. The left (right) panels correspond to normal (inverted) ordering. The dotted line corresponds to the best fit values. The ranges in the filled areas are shown at 1σ , 2σ , and 99% CL.

We plot in Fig. 1 the ranges of the Yukawa couplings $|\tilde{Y}_e|^2 \equiv |Y_1|^2/y^2$ and $|\tilde{Y}_\mu|^2 \equiv |Y_2|^2/y^2$ obtained by projecting the allowed ranges of oscillation parameters from the global analysis of neutrino data [25] using Eqs. (2.22), (2.23), (2.25), and (2.26). The ranges are

shown at 1σ , 2σ , and 99% CL (1dof) while the dotted line corresponds to the best fit values. We show the ranges of these Yukawa couplings as a function of the unknown Majorana phase α , as well as we present the correlation between the Yukawa couplings in the above flavours. As we can see from this figure, the electron and muon Yukawa couplings exhibit a quite different behavior with α for the NO and IO cases. It is also interesting to notice that the two Yukawas are invariant under α going into $\pi - \alpha$ in the limit that s_{13} or δ go to zero for the IO mass ordering.

Also to the same order the Lagrangian for the interactions of the heavy triplet states reads:

$$\begin{aligned}\mathcal{L}_W = & -g \left(\overline{E_1^-} \gamma^\mu N W_\mu^- - \overline{N} \gamma^\mu E_2^+ W_\mu^- \right) + h.c. \\ & - \frac{g}{\sqrt{2}} \left(K_a \overline{\ell_{aL}} \gamma^\mu N_L W_\mu^- + K'_a \overline{\ell_{aL}} \gamma^\mu N_R^c W_\mu^- \right) + h.c. \\ & + g \left(\tilde{K}_a \overline{\nu_{aL}} \gamma^\mu E_{2L}^+ W_\mu^- + \tilde{K}'_a \overline{\nu_{aL}} \gamma^\mu E_{1R}^- W_\mu^- \right) + h.c.\end{aligned}\quad (2.28)$$

$$\begin{aligned}\mathcal{L}_Z = & g C_W \left(\overline{E_1^-} \gamma^\mu E_1^- Z_\mu - \overline{E_2^+} \gamma^\mu E_2^+ Z_\mu \right) \\ & + \frac{g}{2C_W} \left(\tilde{K}_a \overline{\nu_{aL}} \gamma^\mu N_L Z_\mu + \tilde{K}'_a \overline{\nu_{aL}} \gamma^\mu N_R^c Z_\mu \right) + h.c. \\ & + \frac{g}{\sqrt{2}C_W} \left(K_a \overline{\ell_{aL}} \gamma^\mu E_{1L}^- Z_\mu + K'_a \overline{\ell_{aL}} \gamma^\mu E_{2R}^+ Z_\mu \right) + h.c.\end{aligned}\quad (2.29)$$

$$\mathcal{L}_\gamma = e \left(\overline{E_1^-} \gamma^\mu E_1^- A_\mu - \overline{E_2^+} \gamma^\mu E_2^+ A_\mu \right) \quad (2.30)$$

$$\begin{aligned}\mathcal{L}_{h^0} = & \frac{g\Lambda}{2M_W} \left(\tilde{K}_a \overline{\nu_{aL}} N_R + \tilde{K}''_a \overline{\nu_{aL}} N_L^c \right) h^0 + h.c. \\ & + \frac{g\Lambda}{\sqrt{2}M_W} \left(K_a \overline{\ell_{aL}} E_{1R}^- + K''_a \overline{\ell_{aL}} E_{2L}^+ \right) h^0 + h.c. .\end{aligned}\quad (2.31)$$

where c_W is the cosine of the weak mixing angle and the matrices $K^{(\prime)(\prime\prime)}$ and $\tilde{K}^{(\prime)(\prime\prime)}$ are defined as:

$$\begin{aligned}K_a &= -\frac{v}{\sqrt{2}\Lambda} Y_a^* , & \tilde{K}_a &= U_{LEPca}^* K_c , \\ K'_a &= -\frac{v}{\sqrt{2}\Lambda} \left[\epsilon Y_a'^* - \left(\frac{3\mu+\mu'}{4\Lambda} \right) Y_a^* \right] , & \tilde{K}'_a &= U_{LEPca}^* K'_c . \\ K''_a &= -\frac{v}{\sqrt{2}\Lambda} \left[\epsilon Y_a'^* - \left(\frac{\mu-\mu'}{4\Lambda} \right) Y_a^* \right] , & \tilde{K}''_a &= U_{LEPca}^* K''_c .\end{aligned}\quad (2.32)$$

We can see from Eqs. (2.22)–(2.27) that the flavour structure of the lepton number conserving couplings of the heavy triplet fermions, K and \tilde{K} , is fully determined by the low energy neutrino parameters. Moreover, its strength is controlled by the real number yv/Λ while the combination $\epsilon y\hat{y}'/\Lambda$ is fixed by the neutrino masses. On the other hand we find that the L -violating couplings $K^{(\prime)(\prime\prime)}$ and $\tilde{K}^{(\prime)(\prime\prime)}$ are different from the combination determined by the low energy neutrino parameters, \widehat{Y}' . This is, the L -violating couplings of the triplet fermions are not fixed by the low energy neutrino parameters. However one must notice these L -violating couplings are very suppressed since in the MLFV framework the smallness of the neutrino mass naturally stems from the smallness of total lepton number violation which is associated with the smallness of the ϵ , μ and μ' parameters.

The low energy Lagrangian after integrating out the triplet states takes the form of Eq. (1.1) with $\Lambda_{FL} = \Lambda$ and $\Lambda_{LN} = \Lambda/\sqrt{\epsilon}, \Lambda^2/\mu, \Lambda^2/\mu'$. So there is no state with mass

Λ_{LN} . Furthermore the hierarchy of scales $\Lambda_{LN} \gg \Lambda_{FL}$ is technically natural in the t’Hooft’s sense since it is associated with the smallness of ϵ , μ and μ' parameters and in the limit $\mu, \mu', \epsilon \rightarrow 0$ total lepton number symmetry is restored.

In what respects to the phenomenology of the heavy fermion triplets, total lepton number violation appears in their decays as a consequence of the presence of both “primed” and “not primed” couplings in Eqs. (2.28)–(2.31) as well as of the $\mathcal{O}(\mu/\Lambda, \mu'/\Lambda)$ mass splitting and mixing in the heavy states. Thus small total lepton number violation implies a strong hierarchy between the lepton number conserving and lepton number non-conserving effects in the heavy fermion collider phenomenology and renders the observation of L -violating signals impossible at the LHC. This is the main difference with the expected LHC signatures in non MLFV scenarios for type-III see-saw such as the ones studied for example in Refs. [10,12] where $\Delta L = 2$ final states constitute a smoking gun signature which is very suppressed in the MLFV model here considered. Consequently, when discussing the signatures associated with this scenario, we will concentrate on total lepton number conserving signals.

3. Signatures

The dominant production processes for the heavy triplet fermions in this model are pair production due to their gauge interactions:

$$pp \rightarrow E_i^+ E_i^-, \quad pp \rightarrow E_i^\pm N \quad \text{for } i = 1, 2, \quad (3.1)$$

where for simplicity in the second reaction and in what follows we generically denote by “ N ” either the N or \bar{N} state. The cross sections for these processes are well-known functions of their mass, see for example [8], and for completeness we plot them in the left panel of Fig. 2.

The widths for the different decay modes read [8]:

$$\begin{aligned} \Gamma(N \rightarrow \ell_a^- W^+) &= \frac{g^2}{64\pi} |K_a|^2 \frac{\Lambda^3}{M_W^2} \left(1 - \frac{M_W^2}{\Lambda^2}\right) \left(1 + \frac{M_W^2}{\Lambda^2} - 2\frac{M_W^4}{\Lambda^4}\right), \\ \Gamma(N \rightarrow \nu_a Z) &= \frac{g^2}{128\pi c_w^2} |\tilde{K}_a|^2 \frac{\Lambda^3}{M_Z^2} \left(1 - \frac{M_Z^2}{\Lambda^2}\right) \left(1 + \frac{M_Z^2}{\Lambda^2} - 2\frac{M_Z^4}{\Lambda^4}\right), \\ \Gamma(N \rightarrow \nu_a h^0) &= \frac{g^2}{128\pi} |\tilde{K}_a|^2 \frac{\Lambda^3}{M_W^2} \left(1 - \frac{M_{h^0}^2}{\Lambda^2}\right)^2, \\ \Gamma(E_2^+ \rightarrow \nu_a W^+) &= \frac{g^2}{32\pi} |\tilde{K}_a|^2 \frac{\Lambda^3}{M_W^2} \left(1 - \frac{M_W^2}{\Lambda^2}\right) \left(1 + \frac{M_W^2}{\Lambda^2} - 2\frac{M_W^4}{\Lambda^4}\right), \\ \Gamma(E_1^- \rightarrow \ell_a^- Z) &= \frac{g^2}{64\pi c_w^2} |K_a|^2 \frac{\Lambda^3}{M_Z^2} \left(1 - \frac{M_Z^2}{\Lambda^2}\right) \left(1 + \frac{M_Z^2}{\Lambda^2} - 2\frac{M_Z^4}{\Lambda^4}\right), \\ \Gamma(E_1^- \rightarrow \ell_a^- h^0) &= \frac{g^2}{64\pi} |K_a|^2 \frac{\Lambda^3}{M_W^2} \left(1 - \frac{M_{h^0}^2}{\Lambda^2}\right)^2. \end{aligned} \quad (3.2)$$

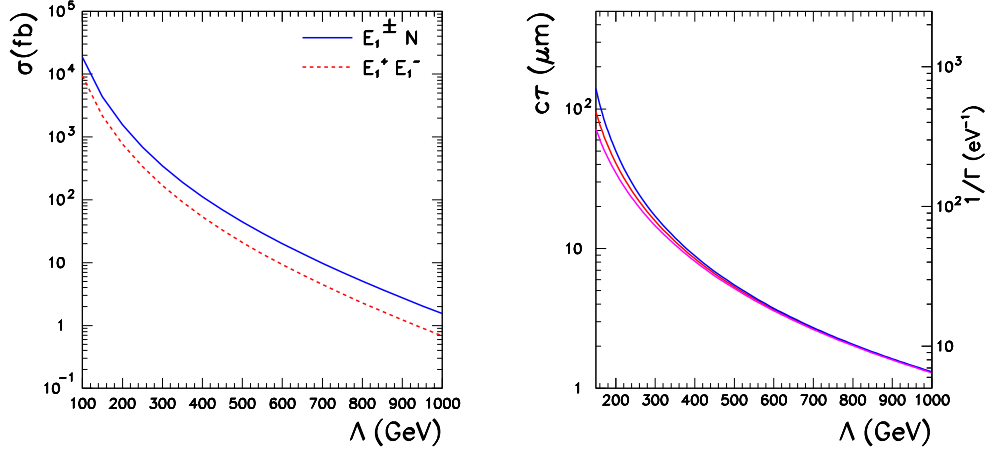


Figure 2: **Left panel:** Cross section for the triplet fermion pair production NE_1^\pm and $E_1^+E_1^-$ that have the same values that the cross sections for NE_2^\pm and $E_2^+E_2^-$ respectively. **Right panel:** Maximum decay length of the triplet fermions E_1^\pm (blue upper curve), N (red middle curve), and E_2^\pm (magenta lower curve). In all cases we have taken $m_{h^0} = 120$ GeV and assumed $k = 1/10$.

Using Eq. (2.32) it is trivial to show that

$$\sum_{a=1}^3 |K_a|^2 = \sum_{a=1}^3 |\tilde{K}_a|^2 = \frac{y^2 v^2}{2\Lambda^2}, \quad (3.3)$$

and show that total decay widths for the three triplet fermions $F = N, E_1^-, E_2^+$ are

$$\Gamma_F^{\text{TOT}} = \frac{g^2 \Lambda^3}{64\pi M_W^2} \frac{y^2 v^2}{\Lambda^2} (1 + \mathcal{F}_F(\Lambda)) \quad (3.4)$$

where $\mathcal{F}_F(\Lambda) \rightarrow 0$ for $\Lambda \gg m_{h^0}, M_Z, M_W$. In a general Type-III see-saw model it is possible that the branching ratio of N or E_i^\pm into a light lepton of a given flavour is vanishingly small. This is not the case for the Type-III see-saw MLFV model studied here since the Yukawa couplings fixed by the neutrino physics are non-vanishing; see Fig. 1.

Other important characteristic of this simple MLFV model is that the values of the neutrino masses imply a lower bound on the total decay width of the triplet fermions as a consequence of the hierarchy between the L -conserving and L -violating y and $\epsilon\hat{y}'$ constants. Let us write $\epsilon\hat{y}' < ky$, where $k < 1$. From Eq. (2.24) or (2.27) it follows that

$$\frac{y^2 v^2}{\Lambda^2} > \frac{m_{3(2)}}{k\Lambda(1+\rho)} = \frac{\sqrt{m_{3(2)}^2 - m_{1(3)}^2}}{k\Lambda(1+\rho)} > \frac{0.046 \text{ eV}}{k\Lambda} \quad (3.5)$$

where the last number is obtained at 99% CL from the global analysis of neutrino data [25]. We depict in the right panel of Fig. 2 the resulting minimum decay width for the triplet fermions as well as their corresponding maximum decay length for any value of $k < 0.1$.

From this figure we see that in this minimal model, even for heavy states as light as $\Lambda = 150$ GeV, the corresponding decay length is always

$$c\tau \lesssim 100 \mu\text{m} \quad (3.6)$$

and it decreases rapidly with Λ . Such a small decay length is too short to produce a detectable displaced decay vertex [26,27]. The use of detached vertices as signatures of the heavy state decays have been discussed in the context of more general see-saw models [9–12]. The lack of this signature in this MLFV model makes the background reduction more challenging. Conversely if a triplet fermion signal is found without a displaced vertex, it will point out towards a very hierarchical neutrino spectrum such as predicted in this simple model.

The most characteristic signature of MLFV Type-III see-saw models is the dependence of the decays of the triplet fermions on the low energy neutrino parameters through the Yukawa couplings. Therefore, in order to be able to tag the lepton flavours, we are lead to consider processes where the new fermions have two-body decays exhibiting charged leptons, *i.e.*

$$pp \rightarrow F(\rightarrow \ell_a X) F'(\rightarrow \ell_b X') \quad (3.7)$$

for $F, F' = N, E_i$ and with $X, X' = Z, W, h^0$. In fact, it turns out that the production cross sections of these processes satisfy

$$\sigma [pp \rightarrow F(\rightarrow \ell_a X) F'(\rightarrow \ell_b X')] \propto |\tilde{Y}_a|^2 |\tilde{Y}_b|^2 \quad (3.8)$$

where $\tilde{Y}_a \equiv \frac{Y_a}{y}$. Therefore, the number of events for final states with different combinations of charged lepton flavours (a, b) can be fully determined in terms of the low-energy neutrino parameters. However, in order to test this prediction one must take into account how the SM bosons, X and X' , decay and that the final state contains at least six particles, what makes the reconstruction of the decay chain non trivial, as well as, the presence of the irreducible SM backgrounds.

Keeping in mind the above discussion, the most promising signatures to both detect the triplet fermions, as well as, to test the flavour predictions in this model are those in which

- (i) The branching ratios into the final state after considering the decays of X, X' are not strongly suppressed.
- (ii) After reconstruction the process should allow us to identify the charged leptons $\ell_{i,j}$ originating from the two body decays of the triplet fermions.
- (iii) To have further information the topology should permit the identification of the bosons X or X' .
- (iv) We should be able to reconstruct the invariant mass of the systems Xl to identify the presence of the triplet fermion pair.

Altogether we find that the most promising final states, that can be fully reconstructed, are three leptons plus two jets and missing energy proceeding via

$$pp \rightarrow W^\pm \rightarrow N(\rightarrow l_a^\mp W^\pm \rightarrow l_a^\mp l_c^\pm \nu) E_1^\pm(\rightarrow \ell_b^\pm Z/h \rightarrow \ell_b^\pm jj), \quad (3.9)$$

and two leptons and four jets resulting from

$$\begin{aligned} pp \rightarrow W^\pm \rightarrow N(\rightarrow \ell_a^\mp W^\pm \rightarrow \ell_a^\mp jj) E_1^\pm(\rightarrow \ell_b^\pm Z/h^0 \rightarrow \ell_b^\pm jj), \\ pp \rightarrow Z/\gamma \rightarrow E_1^\mp(\rightarrow \ell_a^\mp Z/h^0 \rightarrow \ell_a^\mp jj) E_1^\pm(\rightarrow \ell_b^\pm Z/h^0 \rightarrow \ell_b^\pm jj). \end{aligned} \quad (3.10)$$

In order to establish the observability of these signals it is important to keep in mind that the final states present not only SM backgrounds, but also receive contributions from other decays of the triplet fermions, as we shall see. Notice also that we do not consider the production of the charged heavy fermions E_2^\pm since they decay exclusively into νW pairs, so flavour tagging of the final leptons it is not possible. Such processes can contribute to extend the LHC potential to unravel the existence of the triplet fermions but do not allow for the test of the MLFV hypothesis.

We study process (3.9) in detail in Sec. 4. It is characterized by a good signal to background ratio [7] and the main challenges, as we will see, are the reconstruction conditions (ii) and (iv). Process (3.10) is analyzed in Sec. 5. In this case both bosons decay hadronically what gives a high signal rate and since there are only two leptons in the final state and no neutrinos, the reconstruction conditions are more easily fulfilled. The main challenge, as we will see is the presence of a larger QCD background.

We perform our analysis at the parton level, keeping the full helicity structure of the amplitude for both signal and backgrounds. This is achieved using the package MADGRAPH [28] modified to include the new fermions and their couplings. In our calculations we use CTEQ6L parton distribution functions [29] and the MADEVENT default renormalization and factorization scales and a pp center of mass energy $\sqrt{s} = 14$ TeV, unless otherwise stated. Furthermore, we simulate experimental resolutions by smearing the energies, but not directions, of all final state leptons and jets with a Gaussian error given by a resolution $\Delta E/E = 0.14/\sqrt{E}$ for leptons while for jets we assumed a resolution $\Delta E/E = 0.5/\sqrt{E} \oplus 0.03$, if $|\eta_j| \leq 3$ and $\Delta E/E = 1/\sqrt{E} \oplus 0.07$, if $|\eta_j| > 3$ (E in GeV). We also consider a lepton detection efficiency of $e^\ell = 0.9$ and a jet one of $e^j = 0.75$. For simplicity, we assumed the Higgs mass to be 120 GeV in all our analyses.

4. Process $pp \rightarrow \ell\ell\ell jj\cancel{E}_T$

In this section we study the process

$$pp \rightarrow \ell_1^\mp \ell_2^\pm \ell_3^\pm jj\cancel{E}_T \quad (4.1)$$

where we focus on final leptons being either electrons or muons for easier flavour tagging. This final state allow us to look for the events originating from production of triplet fermions in Type-III see-saw models as shown in Eq. (3.9).

The dominant irreducible SM backgrounds are:

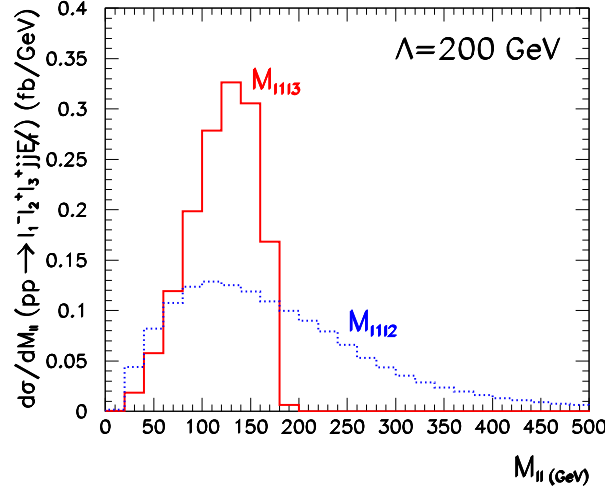


Figure 3: Invariant mass distribution of the two possible opposite-sign equal-flavour lepton pairs for the signal $pp \rightarrow \ell\ell jj \cancel{E}_T$. Here we considered a heavy fermion mass $\Lambda = 200$ GeV.

1. $t\bar{t}W$ production where the two b from $t \rightarrow Wb$ decay are identified as the jets and the three W 's decay leptonically;
2. $t\bar{t}Z$ where the Z decays leptonically while one top decays semi-leptonically and the other decays fully hadronically. Another possibility is that the two top quarks decay semi-leptonically, however, one of the four final state leptons is lost or misidentified. This background can contain up to 4 jets, in addition to the three leptons, of which we require that at least two comply with the acceptance cuts described below; see Eq. (4.2);
3. $WZjj$ and $ZZjj$ with both W and Z decaying leptonically and one lepton in the $ZZjj$ case escapes detection.

In principle the backgrounds from channels containing leptonic Z decays can be reduced by vetoing events where the opposite-sign equal-flavour leptons have invariant mass close to the Z mass [7, 21]. However, as we will see, in this MLFV model signals are large only for relatively light triplet fermions, $\Lambda \leq 500$ GeV, and for these masses the characteristic invariant mass of the opposite-sign equal-flavour lepton pair is not far from the Z mass either. So the Z veto reduces also the signal and no gain in the observability is obtained; for an illustration see Fig. 3. Additional backgrounds, like $t\bar{t}$ and $Zb\bar{b}$, with additional leptons produced from the semi-leptonic decays of the b 's are negligible when no Z veto is applied. Furthermore, we did not take into account reducible backgrounds stemming from the misidentification of a jet as a lepton.

We start our analysis by applying the following acceptance cuts, that are meant to ensure the detection and isolation of the final leptons and jets, as well as a minimum

transverse momentum

$$|\eta_\ell| < 2.5 \quad , \quad |\eta_j| < 3 \quad , \quad \Delta R_{\ell\ell}, \Delta R_{\ell j}, \Delta R_{jj} > 0.4 \quad , \quad p_T^\ell, p_T^j > 20 \text{ GeV} \quad , \quad (4.2)$$

and a minimum missing transverse energy

$$\cancel{E}_T > 10 \text{ GeV} \quad . \quad (4.3)$$

Next, we look for the two jets to be compatible with a Z or a h^0 *i.e.*

$$M_Z - 10 \text{ GeV} < M_{jj} < m_{h^0} + 10 \text{ GeV} \quad . \quad (4.4)$$

Our reconstruction procedure aims to single out events that originate from the reaction (3.9) in order to test the MLFV hypothesis, therefore it is not optimized to get the full LHC potential for the heavy triplet fermion discovery. In order to reconstruct the E_1^\pm and N states we need to identify which of the equal sign leptons $\ell_{2,3}$, is produced in the E_1^\pm two-body decay, as well as, which lepton comes from the W in the N decay chain. To do so we start by reconstructing the two possible values of the invariant mass of each of the equal sign lepton plus two jets, $M_{\ell_{2jj}}$ and $M_{\ell_{3jj}}$. If both $M_{\ell_{2jj}}$ and $M_{\ell_{3jj}}$ are incompatible with the heavy fermion mass, *i.e.*

$$M_{\ell_{2jj}}, M_{\ell_{3jj}} \notin (\Lambda - 40, \Lambda + 40) \text{ GeV} \quad (4.5)$$

the event is discarded. If only one of the two reconstructions is inside this range we consider the corresponding lepton as the one coming from E_1^\pm . If both $M_{\ell_{2jj}}$ and $M_{\ell_{3jj}}$ are inside the range given in Eq. (4.5) we proceed to reconstruct the momentum of the neutrino using that in this final state the neutrino momentum can be reconstructed up to a two-fold ambiguity: its transverse momentum can be directly obtained from momentum conservation in the transverse directions while its longitudinal component can be inferred by requiring that $(p_\nu + p_{\ell_k})^2 = M_W^2$ that leads to

$$p_L^{\nu_{k,n}} = \frac{1}{2p_{\ell_k}^2} \left\{ [M_W^2 + 2(p_T^{\ell_k} \cdot \vec{p}_T)] p_L^{\ell_k} \pm \sqrt{[M_W^2 + 2(p_T^{\ell_k} \cdot \vec{p}_T)]^2 |\vec{p}^\perp|^2 - 4(p_T^{\ell_k} E_{\ell_k} \cancel{E}_T)^2} \right\} \quad (4.6)$$

for $k = 2, 3$ and we label $n = 1, 2$ the solutions with $+, -$ respectively. If neither ℓ_2 nor ℓ_3 lead to a real value of Eq. (4.6), the event is rejected. If only one of them has an acceptable solution we classify this lepton as the one coming from W .

Finally if both leptons lead to satisfactory solutions of Eq. (4.6) we proceed to reconstruct the neutral heavy fermion N . For each $\ell_{2,3}$, and using the two possible solutions for the momentum of the neutrino $p^{\nu_{k,n}}$ ($k = 2, 3$ $n = 1, 2$) we evaluate four invariant masses $M_{\ell_1 \ell_k \nu_{k,n}}$. If for both $k = 2$ and $k = 3$ the two $M_{\ell_1 \ell_k \nu_{k,1}}$ and $M_{\ell_1 \ell_k \nu_{k,2}}$ are outside the interval $(\Lambda - 40, \Lambda + 40) \text{ GeV}$ we do not consider the event. If only $k = 2$ or $k = 3$ has at least one of the corresponding $M_{\ell_1 \ell_k \nu_{k,n}}$ inside this range we select ℓ_k as the one coming from W . Finally, if the ambiguity is still there and both leptons have at least one solution inside this range we cut out the event. In the cases where we identify the leptons before using the reconstruction of the invariant mass of N we also require at the end at least one of the two possible reconstructions to be inside the range $(\Lambda - 40, \Lambda + 40) \text{ GeV}$.

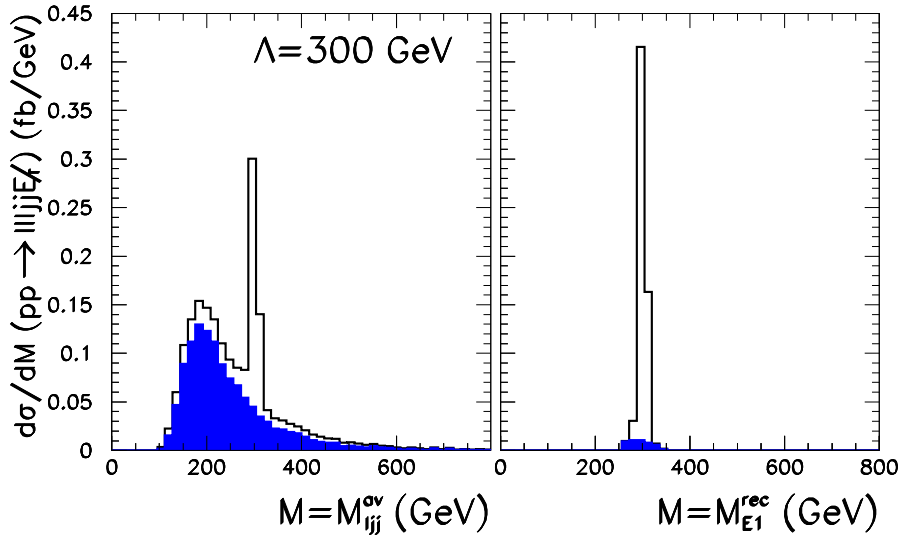


Figure 4: Invariant mass distribution for signal (empty back histogram) and background (filled blue histogram) $M_{\ell jj}$. In the left panel we show the distribution averaged over the two possible combinations with $\ell = \ell_2$ or $\ell = \ell_3$ after imposing the cuts in Eqs. (4.2)–(4.4) and before the reconstruction of the E_1^\pm and N states. On the right panel we show the E_1^\pm reconstructed invariant mass after the selection procedure described in the text. The figure is shown for $\Lambda = 300$ GeV and for characteristic values of the neutrino parameters: $\Delta m_{31}^2 = 2.4 \times 10^{-3}$ eV² (NO), $\Delta m_{21}^2 = 7.65 \times 10^{-5}$ eV², $\sin^2 \theta_{23} = 0.5$, $\sin^2 \theta_{12} = 0.304$ and $\sin^2 \theta_{13} = 0.03$ and vanishing values of the phases $\alpha = \delta_{\text{CP}} = 0$ (for these parameters, $\tilde{Y}_e = 0.37$ and $\tilde{Y}_\mu = 0.84$).

We illustrate the efficiency of this reconstruction procedure in Fig. 4. In the left panel we depict the invariant mass $M_{\ell jj}$ distribution for the signal (empty back histogram) and the background (filled blue histogram) where we averaged over the two possible combinations with $\ell = \ell_2$ or $\ell = \ell_3$. In this plot we imposed the cuts in Eqs. (4.2)–(4.4) before the reconstruction of the E_1^\pm and N states. On the right panel we present the reconstructed invariant mass of the selected combination after the procedure described above. As seen in the figure the procedure selects most of the right combination for the E_1^\pm signal peak while efficiently reducing the background.

In Ref. [21] the ambiguity in the assignment of the equal-sign leptons to the heavy lepton or the W decays was resolved associating to the W decay the lepton that leads to the smallest transverse mass

$$M_T^W = \sqrt{2p_T^{\ell_k} E_T (1 - \cos \Phi_{\ell_k E_T})}, \quad (4.7)$$

where $\Phi_{\ell_k E_T}$ is the angle between the lepton and the missing energy. We verified that this procedure is almost equivalent to ours for high triplet masses Λ . Notwithstanding, for lighter Λ our reconstruction procedure selects more often the correct lepton configuration and after applying the cuts on the invariant masses of N and E_1^\pm it renders a better signal to the background ratio. For example for $\Lambda = 200$ GeV our reconstruction procedure leads

to a misidentification probability of 2% while using only the transverse invariant mass ordering this is increased to 12%.

After cuts and our reconstruction procedure the total cross section of process (3.9) can be written as

$$\sigma_0(2 - \delta_{ab})|\tilde{Y}_a|^2|\tilde{Y}_b|^2$$

when we generate events with the flavour combination ab . As we will shortly see, most of these events are classified as having the correct flavour combination ab by our selection procedure, however, a fraction of them are misidentified and labeled ac for $b \neq c$ with a cross section σ_1 . This happens because we assign wrongly to the triplet fermion a same-sign lepton with a different flavour coming from W . Notice that both classes of events are exclusive since we reject through the reconstruction procedure events that are compatible simultaneously with the ab and ac flavour combinations. Furthermore, Eq. (3.9) is not the only signal process leading to the final state of Eq. (4.1) in the case we have two opposite sign leptons of the same flavour. In this case there are also contributions from:

$$\begin{aligned} pp \rightarrow W^\pm \rightarrow N(\rightarrow \nu_m/\bar{\nu}_m Z \rightarrow \nu_m/\bar{\nu}_m \ell_a^+ \ell_a^-) E_1^\pm(\rightarrow \ell_b^\pm Z/h^0 \rightarrow \ell_b^\pm jj) , \\ pp \rightarrow W^\pm \rightarrow N(\rightarrow \nu_m/\bar{\nu}_m Z/h^0 \rightarrow \nu_m/\bar{\nu}_m jj) E_1^\pm(\rightarrow \ell_b^\pm Z \rightarrow \ell_b^\pm \ell_a^+ \ell_a^-) . \end{aligned} \quad (4.8)$$

It is easy to see that summing over the undetectable neutrino type m the cross section for these processes is proportional to $|\tilde{Y}_b|^2$ and we denoted it by $\sigma_2|\tilde{Y}_b|^2$. These events are classified as aa flavour combination with a cross section $\sigma_3|\tilde{Y}_b|^2$, or as ab with a cross section $(\sigma_2 - \sigma_3)|\tilde{Y}_b|^2$. So altogether the expected signal (S) cross section in each flavour channel is:

$$\begin{aligned} \sigma_{ee}^S &= (\sigma_0 - \sigma_1)|\tilde{Y}_e|^4 + \sigma_1|\tilde{Y}_e|^2|\tilde{Y}_\mu|^2 + \sigma_2|\tilde{Y}_e|^2 + \sigma_3|\tilde{Y}_\mu|^2 , \\ \sigma_{\mu\mu}^S &= (\sigma_0 - \sigma_1)|\tilde{Y}_\mu|^4 + \sigma_1|\tilde{Y}_e|^2|\tilde{Y}_\mu|^2 + \sigma_2|\tilde{Y}_\mu|^2 + \sigma_3|\tilde{Y}_e|^2 , \\ \sigma_{e\mu}^S &= \sigma_1 \left(|\tilde{Y}_e|^4 + |\tilde{Y}_\mu|^4 \right) + 2(\sigma_0 - \sigma_1)|\tilde{Y}_e|^2|\tilde{Y}_\mu|^2 + (\sigma_2 - \sigma_3) \left(|\tilde{Y}_e|^2 + |\tilde{Y}_\mu|^2 \right) , \\ \sigma_{TOT}^S &= \sigma_0 \left(|\tilde{Y}_e|^4 + |\tilde{Y}_\mu|^4 + 2|\tilde{Y}_e|^2|\tilde{Y}_\mu|^2 \right) + 2\sigma_2 \left(|\tilde{Y}_e|^2 + |\tilde{Y}_\mu|^2 \right) . \end{aligned} \quad (4.9)$$

Λ (GeV)	σ_0	σ_1	σ_2	σ_3
150	80.2	2.05	7.53	1.78
200	44.2	0.417	2.20	0.625
300	12.9	0.027	0.125	0.043
500	1.90	$< 10^{-2}$	$< 10^{-2}$	$< 10^{-2}$

Table 1: Contributions to the signal cross sections (σ_{ab}^S) in fb for the processes $pp \rightarrow \ell^\mp \ell^\pm \ell^\pm jj\cancel{E}_T$ for $\ell = e, \mu$ according to Eq. (4.9). The results are presented for different values of the triplet fermion mass Λ and they do not include the detection efficiencies for the leptons and jets.

We present in Table 1 the different contributions to the signal cross section σ_{ab}^S (in fb) after cuts (4.2)–(4.4) and the triplet fermion reconstruction for several values of Λ . As we can see, the bulk of the events passing our cuts originate from correctly reconstructing process (3.9). The SM background cross sections σ_{ab}^B are given in Table 2, where we can see that the dominant SM background is $WZjj$ production.

We are now in position to evaluate the expected number of signal (S) and background (B) events for the $\ell\ell\ell jj\cancel{E}_T$ topology

	$\Lambda = 150\text{GeV}$		$\Lambda = 200\text{GeV}$		$\Lambda = 300\text{GeV}$	
Process	$\sigma_{ee}^B = \sigma_{\mu\mu}^B$	$\sigma_{e\mu}^B$	$\sigma_{ee}^B = \sigma_{\mu\mu}^B$	$\sigma_{e\mu}^B$	$\sigma_{ee}^B = \sigma_{\mu\mu}^B$	$\sigma_{e\mu}^B$
$pp \rightarrow t\bar{t}W$	0.016	0.037	0.021	0.045	0.003	0.005
$pp \rightarrow t\bar{t}Z$	0.082	0.068	0.115	0.074	0.036	0.011
$pp \rightarrow WZjj$	1.66	1.15	1.58	0.950	0.27	0.118
$pp \rightarrow ZZjj$	0.04	0.022	0.046	0.028	0.006	0.002
Total	1.80	1.28	1.76	1.10	0.31	0.14

Table 2: SM background cross sections (σ_{ab}^B) in fb for the processes $pp \rightarrow \ell^\mp \ell^\pm \ell^\pm jj \cancel{E}_T$ with $\ell = e, \mu$. The results are presented for different values of the triplet fermion mass Λ and they do not include the detection efficiencies for the leptons and jets.

with a given flavour combination ab as a function of the neutrino mass and mixing parameters. This can be easily obtained from Eq. (4.9), Table 1, and using the values of the Yukawa couplings in (2.22)–(2.27)

$$N_{ab}^{S,B} = \sigma_{ab}^{S,B} \times \mathcal{L} \times \epsilon, \quad (4.10)$$

where \mathcal{L} is the integrated luminosity and $\epsilon = e^{l^3} \times e^{j^2} = 0.41$ is the detection efficiency for leptons and jets.

Clearly the number of signal events depends on the value of the triplet mass Λ as well as on the neutrino parameters, which we denote here by $\vec{\theta} = (\theta_{12}, \theta_{13}, \theta_{23}, \Delta m_{21}^2, \Delta m_{31}^2, \delta)$ and the Majorana phase α . For example, we present in Fig. 5 the range of predicted number of events in the different flavour combinations for a triplet fermion of mass $\Lambda = 200$ GeV and an integrated luminosity of $\mathcal{L} = 30 \text{ fb}^{-1}$, where the result is shown as a function of the unknown Majorana phase α and the other neutrino parameters $\vec{\theta}$ are obtained from the global analysis of neutrino data [25]. The left (right) panels correspond to normal (inverted) ordering. The ranges are shown for values of $\vec{\theta}$ allowed at 1σ , 2σ , and 99% CL while the dotted line corresponds to the best fit values. The horizontal dashed lines are the corresponding number of SM background events as obtained from Eq. (4.10) with cross sections σ_{ab}^B in Table 2.

It is important to notice from Fig. 5 that the two neutrino mass orderings lead to a quite distinct dependence of N_{ee}^S , $N_{\mu\mu}^S$, and $N_{e\mu}^S$ with the Majorana phase α . Since the SM background is rather small compared to the expected signal, we might be able to determine the neutrino ordering by simply comparing the three different number of events for basically all values of α as well as to obtain information on the value of α . We will go back to this point at the end of next section.

Next we study the observability of this MLFV model as a function of the triplet fermion mass Λ , the range of the neutrino parameters $\vec{\theta}$ and the Majorana phase α . We estimate the significance of the signal by constructing a simple χ^2 function in terms of the three

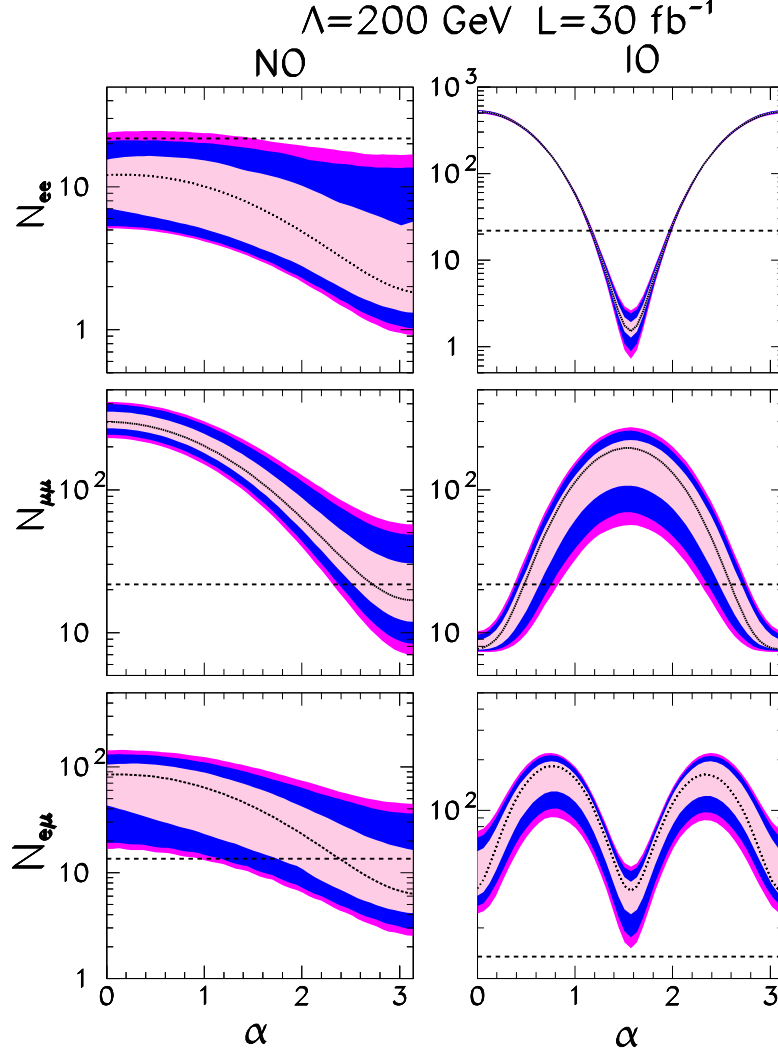


Figure 5: Predicted number of events N_{ab} for $pp \rightarrow \ell^\pm \ell^\mp \ell^\mp jj \cancel{E}_T$ with $\ell = e, \mu$ for a triplet fermion of mass $\Lambda = 200 \text{ GeV}$ with an integrated luminosity of $\mathcal{L} = 30 \text{ fb}^{-1}$. The horizontal dashed lines are the corresponding number of background events; see Table 2. The conventions are the same as in Fig. 1.

signal and background flavour rates for a given value of Λ

$$\chi^2(\vec{\theta}, \alpha) = \sum_{ab=ee, e\mu, \mu\mu} \chi_{ab}^2(\vec{\theta}, \alpha), \quad (4.11)$$

$$\chi_{ab}^2(\vec{\theta}, \alpha) = \frac{N_{ab}^{S^2}}{N_{ab}^B} \quad \text{For } N_{ab}^B \geq 10,$$

$$\chi_{ab}^2(\vec{\theta}, \alpha) = 2(N_{ab}^S + N_{ab}^B \ln \frac{N_{ab}^B}{N_{ab}^B + N_{ab}^S}) \quad \text{For } N_{ab}^B < 10.$$

Figure 6 shows the significance – estimated as $\sqrt{\chi^2}$ – of the excess of signal events $pp \rightarrow \ell^\pm \ell^\mp \ell^\mp jj \cancel{E}_T$ for three values of the mass Λ and for $\mathcal{L} = 30 \text{ fb}^{-1}$ as a function of the

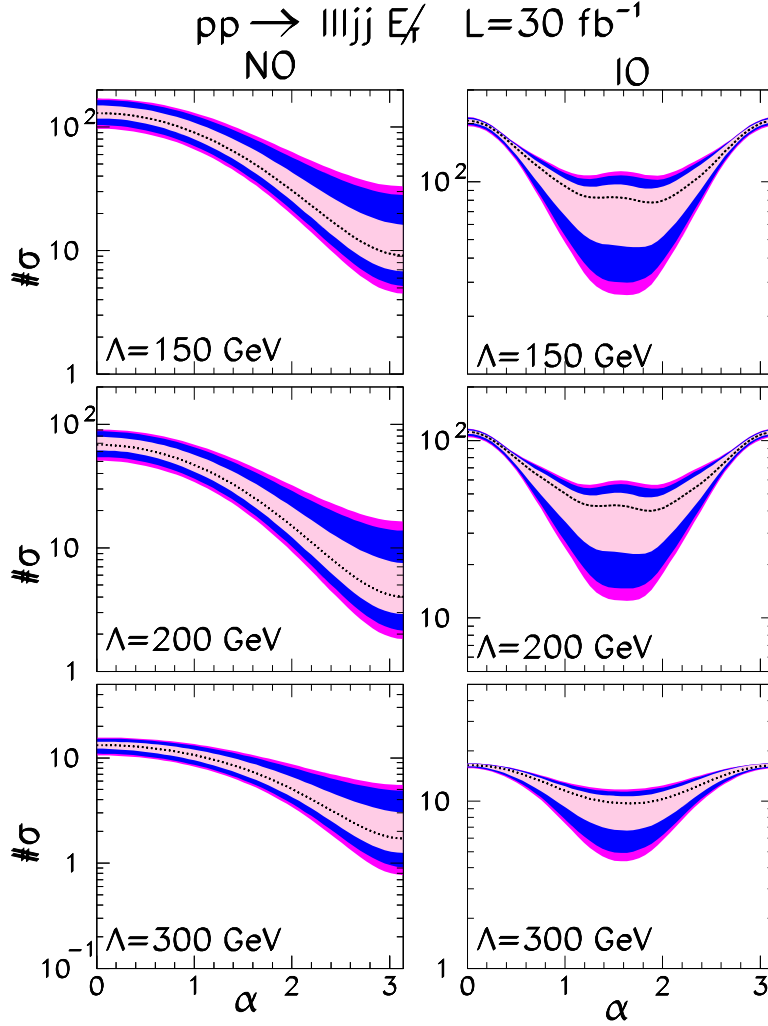


Figure 6: Signal significance ($\# \sigma$) in the channel $pp \rightarrow \ell^\pm \ell^\mp \ell^\mp jj \cancel{E}_T$ with $\ell = e, \mu$ for three triplet fermion masses and for an integrated luminosity of $\mathcal{L} = 30 \text{ fb}^{-1}$ as function of the Majorana phase α . The conventions are the same as in Fig. 1.

Majorana phase α . The significance is shown as obtained for the best fit values of $\vec{\theta}$ (dashed line) and 1σ , 2σ , and 99% CL ranges of $\vec{\theta}$ (filled areas) obtained from the global analysis of neutrino data [25]. The left (right) panels correspond to normal (inverted) ordering.

As long as the number of background events is large enough, the results for other luminosities can be simply obtained by rescaling figure 6 by a factor $1/\sqrt{\mathcal{L}/30}$. From this figure we see that with $\mathcal{L} = 100 \text{ fb}^{-1}$ LHC can discover/discard this MLFV model using this channel in most of the presently allowed neutrino parameter space for $\Lambda \leq 300 \text{ GeV}$. In some parts of the neutrino parameter space, and in particular if the neutrino masses have inverse ordering, the reach can be extended to higher masses or to a pp center-of-mass energy $\sqrt{s} = 7 \text{ TeV}$ as we will discuss in Sec.6.

5. Process $pp \rightarrow \ell\ell jjjj$

The search for Type-III see-saw leptons via process (3.10), *i.e.*

$$pp \rightarrow \ell_1^\mp \ell_2^\pm jjjj \quad (5.1)$$

with $\ell_{1(2)} = e, \mu$ does not present ambiguities in the flavour tagging, what favors the test of the MLFV hypothesis. However, it is plagued with a large SM background. The dominant backgrounds for this process are:

- $t\bar{t}jj$ production where the two b 's from the $t \rightarrow Wb$ decays are identified as jets and both W 's decay leptonically;
- Z^*/γ^*jjjj with the Z^*/γ^* leading to a charged lepton pair. Notice that this process only contributes to the final state with equal flavour leptons.

Additional backgrounds include $t\bar{t}W$ and $t\bar{t}Z$ but after the reconstruction requirements they are very much suppressed. For further details see Refs. [7, 10] for a detailed analysis of the backgrounds for this signature².

Our analysis starts by applying the acceptance and isolation cuts for the final leptons and jets, as well as the minimum transverse momentum requirement as described in Eq. (4.2). Since the signal does not contain any undetectable particle we further required a maximum amount of missing energy in the event

$$\cancel{E}_T < 30 \text{ GeV} . \quad (5.2)$$

In what respects the reconstruction of the triplet fermions, there are six possible ways of grouping the leptons and jets in the final state in two sets of one lepton and two jets. We impose that at least one of the six combinations has the two invariant masses inside the triplet fermion mass region

$$\Lambda - 40 \text{ GeV} < M_{\ell jj} < \Lambda + 40 \text{ GeV}. \quad (5.3)$$

Furthermore the corresponding invariant masses of the two jet pairs are required to verify

$$M_W - 10 \text{ GeV} < M_{jj} < m_{h^0} + 10 \text{ GeV}. \quad (5.4)$$

Since there is no ambiguity in the assignment of the two charged leptons the total cross section of process (3.10) is simply given by

$$\sigma_{ab}^S = \sigma_4(2 - \delta_{ab})|\tilde{Y}_a|^2|\tilde{Y}_b|^2 . \quad (5.5)$$

Even after the reconstruction of the invariant masses of the two triplet fermions, the SM backgrounds are still large, in particular the one arising from Z^*/γ^*jjjj . To further reduce

²We employ the latest version of MadEvent MG5 [30] in the evaluation of these backgrounds. For the Z^*/γ^*jjjj process MG5 gives a 20-30% larger value of this background after all the cuts are imposed as compared to previous versions of MadEvent.

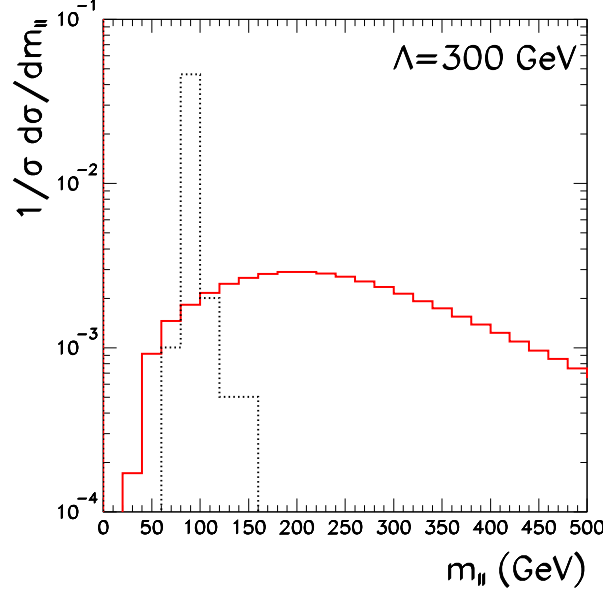


Figure 7: Distribution of the charged lepton pair invariant mass for the signal (solid red histogram) and Z^*/γ^*jjjj background (dotted black histogram) after cuts (4.2), (5.2), (5.3) and (5.4), and for a heavy fermion mass $\Lambda = 300$ GeV.

this background we make use of the fact that in the signal the characteristic invariant mass of the two leptons is larger than for the background as illustrated in Fig. 7. Consequently, this background is reduced by factor 20–8 for $\Lambda = 150$ –500 GeV if we impose that the invariant mass of the two charged leptons verify

$$M_{\ell^+\ell^-} > 100 \text{ GeV}. \quad (5.6)$$

We present in Table 3 the cross sections for signal and SM backgrounds after cuts (4.2), (5.2), (5.3), (5.4), and (5.6). The predicted number of events for the triplet fermion signal in this channel for the different flavour combinations can be easily obtained from Eq. (4.10) and Table 3 using the values of the Yukawa couplings in (2.22)–(2.27) and a detection efficiency of $\epsilon = e^{j^4} \times e^{\ell^2} = 0.26$.

We plot in Fig. 8 the range of the expected number of events in the different flavour combinations as a function of the unknown Majorana phase α for a triplet fermion of mass $\Lambda = 500$ GeV and an integrated luminosity of $\mathcal{L} = 30 \text{ fb}^{-1}$. The ranges are shown at 1σ , 2σ , and 99% CL from the global analysis of neutrino data [25], while the dotted line corresponds to the best fit values. The left (right) panels correspond to normal (inverted) ordering while the horizontal dashed lines stand for the predicted number of SM background events. Here again, we can see that the dependence of N_{ee}^S , $N_{\mu\mu}^S$, and $N_{e\mu}^S$ on the CP violating Majorana phase α are quite distinct for NO and IO.

The observability of this MLFV model in the $\ell\ell jjjj$ channel is depicted in Fig. 9 where we show the signal significance as a function of the Majorana phase α for different CL of

	Signal (fb)	Background (fb)	
		$t\bar{t}jj$	Z^*/γ^*jjjj
$\Lambda(\text{GeV})$	σ_4	$\sigma_{ee}^B = \sigma_{\mu\mu}^B = \sigma_{e\mu}^B/2.$	$\sigma_{ee}^B = \sigma_{\mu\mu}^b$
150	276.0	6.0	29.3
200	216.0	9.7	33.2
300	74.9	0.89	4.6
500	11.3	0.018	0.057

Table 3: Signal and background cross sections for $pp \rightarrow \ell_a^\mp \ell_b^\pm jjjj$ after cuts (4.2),(5.2), (5.3), (5.4), and (5.6) for different values of the triplet fermion mass Λ . These results do not include detection efficiencies for leptons and jets.

the neutrino parameters. Like the previous analysis, we added the flavours combinations to define the signal significance. Comparing Figs. 6 and 9 we can see that after the background reduction achieved by the mass reconstruction conditions Eqs.(5.3) and (5.4) and the lepton pair invariant mass cut (5.6), the channel $\ell\ell jjjj$ offers better potential statistical sensitivity for the discovery or exclusion of this MLFV model in particular for heavier masses Λ , despite its still larger SM backgrounds. One must keep in mind, however, that the final attainable precision depends on the systematic background uncertainties which are expected to be larger for this channel [7].

We can see from Figs. 5 and 8 that the two neutrino orderings lead to a very distinct dependence of N_{ee}^S , $N_{\mu\mu}^S$, and $N_{e\mu}^S$ as a function of α for both final states. It is particularly striking the upper right panels that presents a very narrow range for the ee flavour combination for inverted ordering and a fixed value of α . Thus one expects to be able to discriminate between the inverted and normal ordering of the neutrino masses studying the correlations between the different flavour combinations for a large fraction of the values of the unknown phase α , or even to determine its value.

To illustrate this point we have assumed that the observed number of events in the three flavour combinations for both $pp \rightarrow \ell\ell jj\cancel{E}_T$ and $pp \rightarrow \ell\ell jjjj$ are those predicted for a given mass Λ (assumed to be independently determined) in the NO for the best value of oscillation parameters $\bar{\theta}_b$ and for some fix value of the Majorana phase $\bar{\alpha}$ plus the expected background events, *i.e.* $N_i^{\text{obs}}(\bar{\theta}_b, \bar{\alpha}) = N_i^S(\bar{\theta}_b, \bar{\alpha}) + N_i^B$ with $i = 1, 6$ corresponding to $ee, e\mu, \mu\mu$ for the two processes. We then try reconstruct the ordering and value of $\bar{\alpha}$ by fitting those six rates N_i^{obs} in either NO or IO with different values of $\vec{\theta}$ (within their 95%

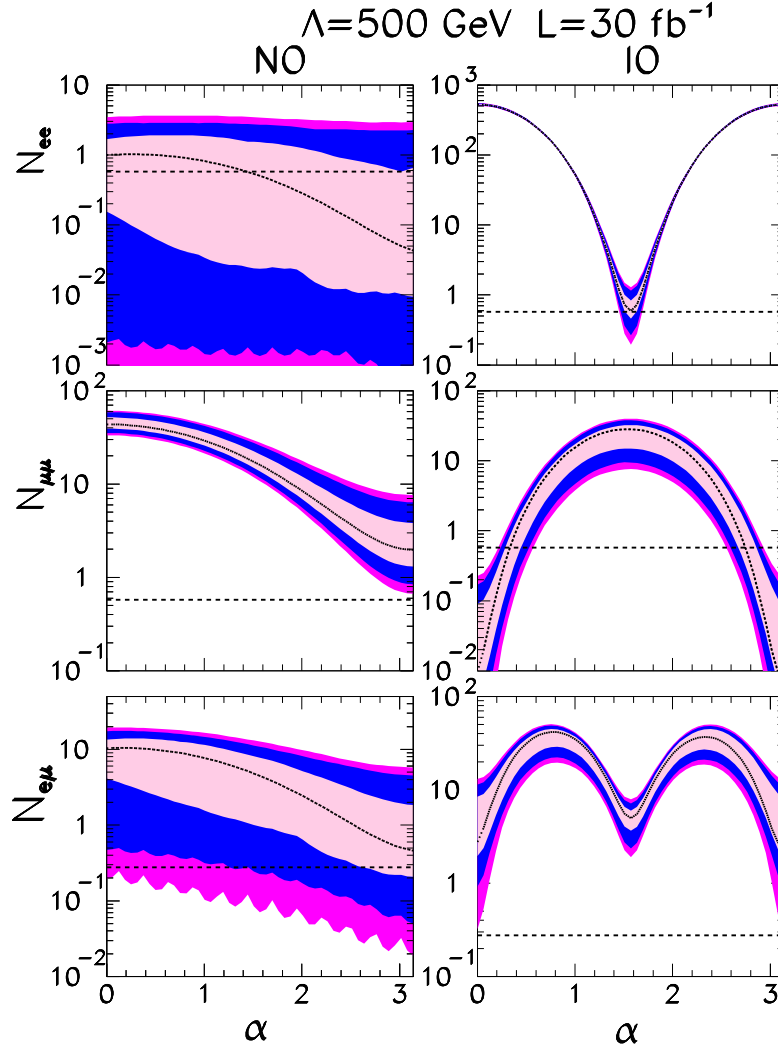


Figure 8: Predicted number of events N_{ab} for $pp \rightarrow \ell_a^\pm \ell_b^\mp jjjj$ for a triplet fermion of mass $\Lambda = 500 \text{ GeV}$ with an integrated luminosity of $\mathcal{L} = 30 \text{ fb}^{-1}$. The horizontal dashed lines are the corresponding number of background events. The conventions are the same as in Fig. 1.

CL allowed region from oscillations) and α . In order to do so we define

$$\chi_{min}^2(\alpha) = \min_{\vec{\theta} \in 95\% \text{CL}} \sum_{i=1,6} \chi_i^2(\vec{\theta}, \alpha) \quad (5.7)$$

$$\chi_i^2(\vec{\theta}, \alpha) = \frac{\left[N_i^S(\vec{\theta}, \alpha) + N_i^B - N_i^{\text{obs}}(\bar{\theta}_b, \bar{\alpha}) \right]^2}{N_i^{\text{obs}}(\bar{\theta}_b, \bar{\alpha})} \quad \text{for } N_i^{\text{obs}}(\bar{\theta}_b, \bar{\alpha}) \geq 10 ,$$

$$\chi_i^2(\vec{\theta}, \alpha) = 2 \left[N_i^S(\vec{\theta}, \alpha) + N_i^B - N_i^{\text{obs}}(\bar{\theta}_b, \bar{\alpha}) + N_i^{\text{obs}}(\bar{\theta}_b, \bar{\alpha}) \ln \frac{N_i^{\text{obs}}(\bar{\theta}_b, \bar{\alpha})}{N_i^S(\vec{\theta}, \alpha) + N_i^B} \right] \quad \text{for } N_i^{\text{obs}}(\bar{\theta}_b, \bar{\alpha}) < 10 .$$

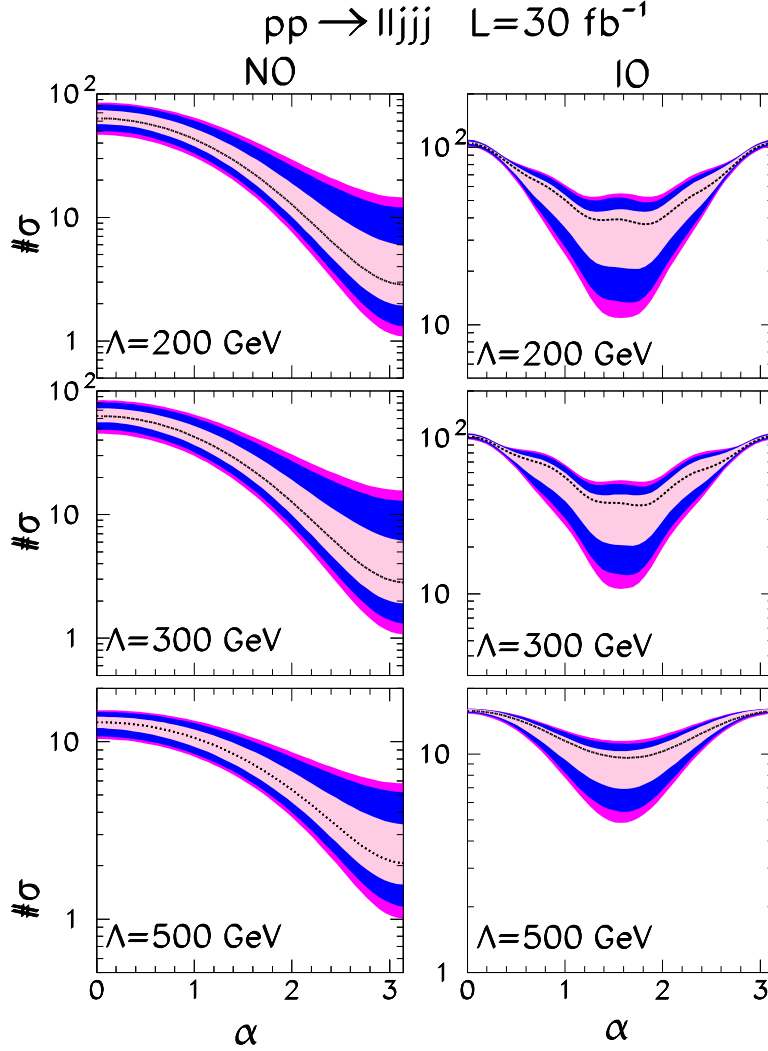


Figure 9: Expected significance $\# \sigma$ of signal versus background events for $pp \rightarrow \ell_a^\pm \ell_b^\mp jjjj$ for three triplet fermion masses and for an integrated luminosity of $\mathcal{L} = 30 \text{ fb}^{-1}$. The conventions are the same as in Fig. 1.

We plot in Fig. 10 $\chi_{\min}^2(\alpha)$ for three values of $\bar{\alpha} = 0, \frac{\pi}{2}, \text{ and } \pi$. Clearly for the panels in the left which corresponds to the NO $\chi_{\min}^2(\alpha)$ presents a minimum for $\alpha = \bar{\alpha}$. The panels on the right show for which cases the event rates simulated could also be predicted by IO with a somewhat different value of α . Whenever one of the curves do not appear in the right panels it is because the corresponding $\chi_{\min}^2(\alpha) > 20$ for all values of α .

Figure 10 illustrates that for masses $\Lambda \lesssim 200 \text{ GeV}$ it is possible to discriminate between NO and IO except for $\bar{\alpha} \sim \frac{\pi}{2}$. Furthermore in those cases for which discrimination between NO and IO is possible one also obtains information on the value of $\bar{\alpha}$. As the mass increases it becomes harder to disentangle IO and NO, and for 500 GeV for any value of simulated $\bar{\alpha}$ there is always a value of α for which the expected rates in IO mimic the simulated ones in NO at better than $\sim 2\sigma$.

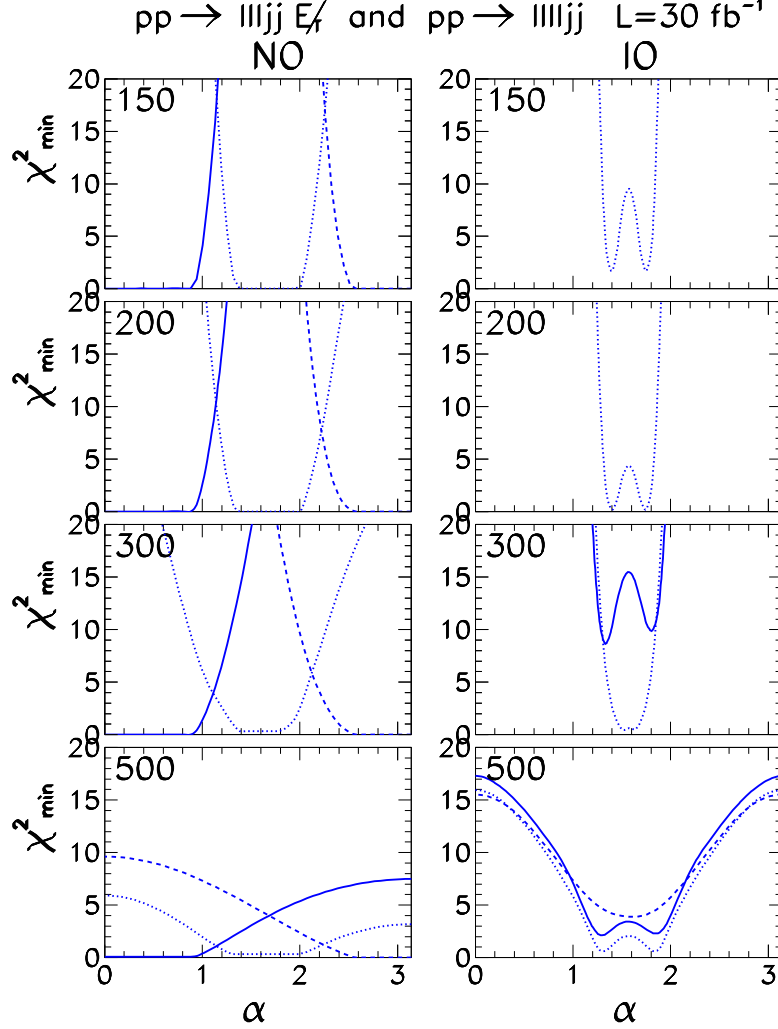


Figure 10: $\chi^2_{\min}(\alpha)$ defined in Eq. (5.8). The full, dotted and dashed lines correspond to a simulated value of the event rates in NO for best fit values of oscillation parameters and $\bar{\alpha} = 0, \frac{\pi}{2}, \pi$ respectively. Whenever one of the curves do not appear in the right panels it is because the corresponding $\chi^2_{\min}(\alpha) > 20$ for all values of α .

6. Signals at 7 TeV

The present LHC run with a center-of-mass energy of 7 TeV has been very successful exhibiting a rapidly increasing integrated luminosity. Therefore, we present in this section the prospective LHC reach for this run. We analyzed the $pp \rightarrow \ell\ell jj E_T$ signal at 7 TeV applying the cuts defined in Eqs. (4.2)–(4.4), as well as, our reconstruction procedure described in Sect. 4. We display in Table 4 the contributions to the signal cross sections (σ_{ab}^S) for the processes $pp \rightarrow \ell^\mp \ell^\pm \ell^\pm jj E_T$ for $\ell = e, \mu$ according to Eq. (4.9). As we can see, the reconstruction efficiency and the misidentification are at the approximately same level for the 7 and 14 TeV runs. Of course, the signal cross section at 7 TeV is a factor 2–4

	$pp \rightarrow \ell^\mp \ell^\pm \ell^\pm jj\cancel{E}_T$				$pp \rightarrow \ell_a^\mp \ell_b^\pm jjjj$
Λ (GeV)	σ_0	σ_1	σ_2	σ_3	σ_4
150	33.2	0.958	3.25	0.820	111
200	16.3	0.176	0.852	0.259	78.4
300	3.72	0.009	0.036	0.013	21.0

Table 4: Contributions to the signal cross sections (σ_{ab}^S) in fb for the processes $pp \rightarrow \ell^\mp \ell^\pm \ell^\pm jj\cancel{E}_T$ and $pp \rightarrow \ell_a^\mp \ell_b^\pm jjjj$ for $\ell = e, \mu$ according to Eq. (4.9) and Eq. (5.5) for a 7 TeV center-of-mass energy. These results do not include the detection efficiencies for the leptons and jets.

	$\Lambda = 150\text{GeV}$		$\Lambda = 200\text{GeV}$		$\Lambda = 300\text{GeV}$	
Process	$\sigma_{ee}^B = \sigma_{\mu\mu}^B$	$\sigma_{e\mu}^B$	$\sigma_{ee}^B = \sigma_{\mu\mu}^B$	$\sigma_{e\mu}^B$	$\sigma_{ee}^B = \sigma_{\mu\mu}^B$	$\sigma_{e\mu}^B$
$pp \rightarrow t\bar{t}W$	0.0073	0.0129	0.0074	0.0147	0.0010	0.0017
$pp \rightarrow t\bar{t}Z$	0.0187	0.0143	0.0214	0.0161	0.0057	0.0017
$pp \rightarrow WZjj$	0.5653	0.3656	0.5475	0.3053	0.0709	0.0336
$pp \rightarrow ZZjj$	0.0138	0.0107	0.0133	0.0082	0.0012	0.0007
Total ($\ell\ell jj\nu$)	0.605	0.403	0.590	0.344	0.079	0.038
$pp \rightarrow t\bar{t}jj$	1.30	2.60	1.93	3.86	0.15	0.30
$pp \rightarrow Z^*/\gamma^* jjjj$	10.3	0	11.3	0	0.26	0
Total ($\ell jjjj$)	11.60	2.60	13.23	3.86	0.41	0.30

Table 5: SM background cross sections (σ_{ab}^B) in fb for the processes $pp \rightarrow \ell^\mp \ell^\pm \ell^\pm jj\cancel{E}_T$ and $pp \rightarrow \ell_a^\mp \ell_b^\pm jjjj$ for $\ell = e, \mu$ and a 7 TeV center-of-mass energy. The results are presented for different values of the triplet fermion mass Λ and they do not include the detection efficiencies for the leptons and jets.

smaller than at 14 TeV.

We present in Table 5 the main irreducible backgrounds for the $\ell\ell jj\cancel{E}_T$ channel after cuts and our reconstruction procedure but without including detection efficiencies. As we can see the most severe background is again the $WZjj$ production with cross sections of the order of 0.5 fb or smaller depending on Λ . Therefore, for integrated luminosities of the order of 10 fb^{-1} we can anticipate a handful of background and signal events for light triplet fermions, *i.e.* $\Lambda \lesssim 200 \text{ GeV}$.

We also analyzed the $\ell jjjj$ channel at 7 TeV applying the cuts and reconstruction procedure stated in Eqs. (4.2) and (5.2)–(5.4). The signal and background cross sections after cuts without including the detection efficiencies are presented in Tables 4 and 5. Once more, the most relevant background for equal flavour leptons is $Z^*/\gamma^* jjjj$ production while the $t\bar{t}jj$ process is dominant for different flavour leptons.

Figure 11 depicts the significance of the signal versus background for different values of the heavy fermion mass and assuming the same detection efficiencies than for 14 TeV and an integrated luminosity of 10 fb^{-1} . To compensate for the smaller statistics the event rates for the three flavour channels have been added for each of the two processes and the significances for two total event rates have been combined. As before, the predictions are shown as obtained for the best fit (dashed line) and 1σ , 2σ , and 99% CL neutrino

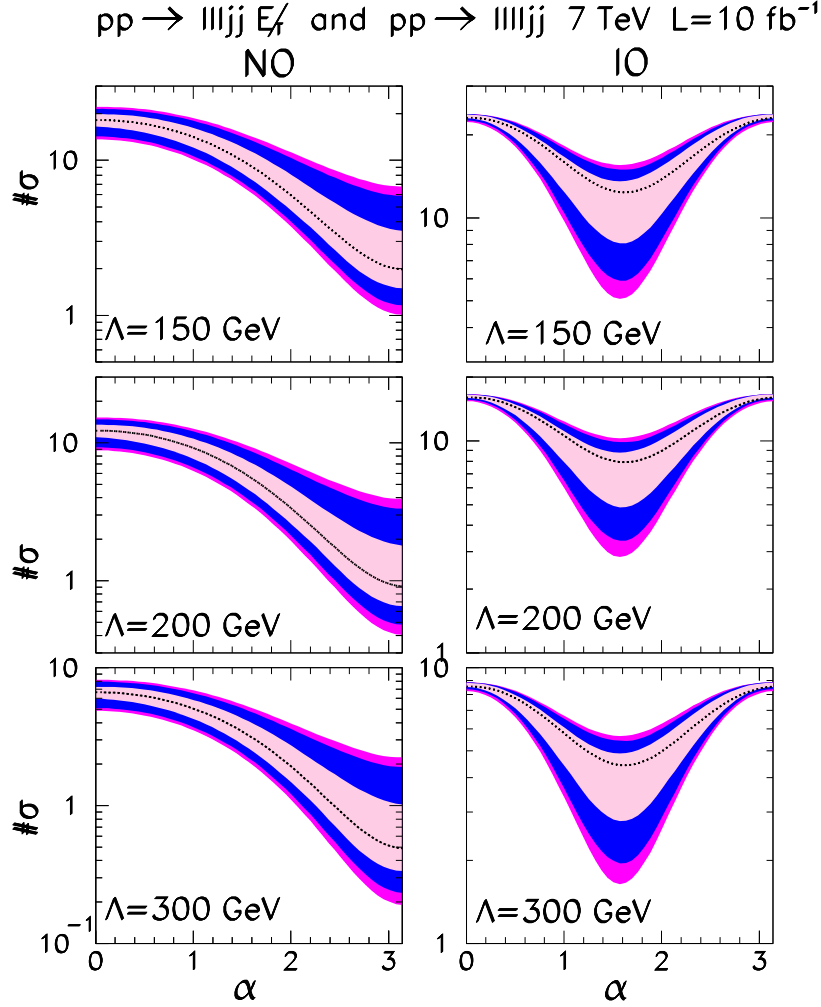


Figure 11: Expected significance $\#\sigma$ of signal versus background events for a center-of-mass energy of 7 TeV and assuming the detection efficiencies used in the 14 TeV analyses. The conventions are the same as in Fig. 1.

parameter ranges (filled areas) obtained from the global analysis of neutrino data [25]. We can see from this figure that integrated luminosities of the order of 10 fb^{-1} can lead to the discovery of the new heavy fermions in a significant range of α for masses $\Lambda \lesssim 200 \text{ GeV}$.

7. Summary and discussions

In this work we have analyzed the signal of Type-III see-saw models with MLFV taking into account the constraints emanating from low energy neutrino data. We have presented our results as a function of the Majorana phase α for the best fit and 1σ , 2σ , and 99% CL neutrino parameter ranges obtained from the global analysis of neutrino data [25]. We have optimized the analysis for a center-of-mass energy of 14 TeV, however in Sec.6 we have

also studied the potential of the LHC running at 7 TeV and with integrated luminosity $\mathcal{O}(10) \text{ fb}^{-1}$ to probe part of the parameter space of this model.

After careful analyses of the signal and SM backgrounds we have established that mass scales of the order of 300 (500) GeV can be probed in the channel $\ell\ell jj\cancel{E}_T$ ($\ell\ell jjjj$). It is interesting to notice that the $\ell\ell jjjj$ final state can be the best discover channel for triplet fermions at the LHC if their larger SM backgrounds are well understood. Moreover, once a signal of Type-III see-saw models with MLFV is observed its energy scale Λ can be precisely determined by measuring the mass of the new heavy fermions; as an illustration see Fig. 4. One very clean channel for this determination is the production of the charged lepton E_1^\pm followed by its decay into three leptons, provided there will be enough integrated luminosity available.

Finally let us comment that the discovery at the LHC of the triplet fermions predicted by MLFV Type-III see-saw models is not only important for unraveling the mechanism responsible for the tiny observed neutrino masses, but it may also allow for the determination of the ordering of the neutrino masses. In fact, the ratio of the flavour combinations ee , $\mu\mu$, and $e\mu$ can discriminate between inverted and normal ordering as we can see from Figs. 5, 8 and 10.

Acknowledgments

We thank E. Nardi for comments. M.C. G-G thanks the CERN Theory group for their hospitality and her collaborators in the neutrino oscillation analysis M. Maltoni and J. Salvado. O.J.P.E is supported in part by Conselho Nacional de Desenvolvimento Científico e Tecnológico (CNPq) and by Fundação de Amparo à Pesquisa do Estado de São Paulo (FAPESP); M.C.G-G is also supported by USA-NSF grant PHY-0653342, by CUR Generalitat de Catalunya grant 2009SGR502 and together with J.G-F by MICINN FPA2010-20807 and consolider-ingenio 2010 program CSD-2008-0037. J.G-F is further supported by Spanish ME FPU grant AP2009-2546.

References

- [1] For a review on neutrino physics, see for example M. C. Gonzalez-Garcia, M. Maltoni, Phys. Rept. **460**, 1-129 (2008). [arXiv:0704.1800 [hep-ph]].
- [2] S. Weinberg, Phys. Rev. Lett. **43** (1979) 1566.
- [3] P. Minkowski, Phys. Lett. B **67** (1977) 421; T. Yanagida, in *Proceedings of the Workshop on the Unified Theory and the Baryon Number in the Universe*, eds. O. Sawada et al., (KEK Report 79-18, Tsukuba, 1979), p. 95; M. Gell-Mann, P. Ramond and R. Slansky, in *Supergravity*, eds. P. van Nieuwenhuizen et al., (North-Holland, 1979), p. 315; R. N. Mohapatra and G. Senjanović, Phys. Rev. Lett. **44** (1980) 912.
- [4] W. Konetschny and W. Kummer, Phys. Lett. B **70** (1977) 433; T. P. Cheng and L. F. Li, Phys. Rev. D **22** (1980) 2860; G. Lazarides, Q. Shafi and C. Wetterich, Nucl. Phys. B **181** (1981) 287; J. Schechter and J. W. F. Valle, Phys. Rev. D **22** (1980) 2227; R. N. Mohapatra and G. Senjanović, Phys. Rev. D **23** (1981) 165.

- [5] R. Foot, H. Lew, X. G. He and G. C. Joshi, Z. Phys. C **44** (1989) 441.
- [6] E. Ma, Phys. Rev. Lett. **81** (1998) 1171 [arXiv:hep-ph/9805219]; B. Bajc and G. Senjanović, JHEP **0708** (2007) 014 [arXiv:hep-ph/0612029]; P. Fileviez Pérez, Phys. Lett. B **654** (2007) 189 [arXiv:hep-ph/0702287];
- [7] F. del Aguila and J. A. Aguilar-Saavedra, Nucl. Phys. B **813** (2009) 22 [arXiv:0808.2468 [hep-ph]].
- [8] F. del Aguila and J. A. Aguilar-Saavedra, Phys. Lett. B **672** (2009) 158 [arXiv:0809.2096 [hep-ph]].
- [9] P. Fileviez Perez, T. Han, G. -y. Huang, T. Li, K. Wang, Phys. Rev. **D78**, 015018 (2008). [arXiv:0805.3536 [hep-ph]].
- [10] R. Franceschini, T. Hambye, A. Strumia, Phys. Rev. **D78**, 033002 (2008). [arXiv:0805.1613 [hep-ph]].
- [11] T. Li, X. -G. He, Phys. Rev. **D80**, 093003 (2009). [arXiv:0907.4193 [hep-ph]].
- [12] A. Arhrib, B. Bajc, D. K. Ghosh, T. Han, G. -Y. Huang, I. Puljak, G. Senjanovic, Phys. Rev. **D82**, 053004 (2010). [arXiv:0904.2390 [hep-ph]]; B. Bajc, M. Nemevsek, G. Senjanovic, Phys. Rev. **D76** (2007) 055011. [hep-ph/0703080].
- [13] R. N. Mohapatra and J. W. F. Valle, Phys. Rev. D **34** (1986) 1642.
- [14] J. Kersten, A. Y. Smirnov, Phys. Rev. **D76** (2007) 073005. [arXiv:0705.3221 [hep-ph]].
- [15] M. B. Gavela, T. Hambye, D. Hernandez and P. Hernandez, JHEP **0909** (2009) 038 [arXiv:0906.1461 [hep-ph]].
- [16] V. Cirigliano, B. Grinstein, G. Isidori and M.B. Wise, Nucl. Phys. B **728** (2005) 121.
- [17] S. Davidson and F. Palorini, Phys. Lett. B **642** (2006) 72 [arXiv:hep-ph/0607329].
- [18] R. Alonso, G. Isidori, L. Merlo, L. A. Munoz, E. Nardi, JHEP **1106** (2011) 037. [arXiv:1103.5461 [hep-ph]].
- [19] R. S. Chivukula and H. Georgi, Phys. Lett. B **188** (1987) 99. A. J. Buras, P. Gambino, M. Gorbahn, S. Jager and L. Silvestrini, Phys. Lett. B **500**, 161 (2001) [arXiv:hep-ph/0007085]. G. D'Ambrosio, G. F. Giudice, G. Isidori and A. Strumia, Nucl. Phys. B **645**, 155 (2002) [arXiv:hep-ph/0207036].
- [20] J. Garayoa and T. Schwetz, JHEP **0803**, 009 (2008) [arXiv:0712.1453 [hep-ph]].
- [21] E. Gross, D. Grossman, Y. Nir, O. Vitells, Phys. Rev. **D81**, 055013 (2010). [arXiv:1001.2883 [hep-ph]].
- [22] J. Schechter and J. W. F. Valle, Phys. Rev. D **21** (1980) 309.
- [23] S. Antusch, C. Biggio, E. Fernandez-Martinez, M. B. Gavela, J. Lopez-Pavon, JHEP **0610**, 084 (2006). [hep-ph/0607020].
- [24] A. Abada, C. Biggio, F. Bonnet, M. B. Gavela and T. Hambye, JHEP **0712** (2007) 061 [arXiv:0707.4058 [hep-ph]].
- [25] M. C. Gonzalez-Garcia, M. Maltoni, J. Salvado, JHEP **1004**, 056 (2010). [arXiv:1001.4524 [hep-ph]].
- [26] G. Aad *et al.* [ATLAS Collaboration], JINST **3**, S08003 (2008).

- [27] R. Adolphi *et al.* [CMS Collaboration], JINST **3** (2008) S08004.
- [28] T. Stelzer and F. Long, Comput. Phys. Commun. **81** (1994) 357; [arXiv:hep-ph/9401258].
F. Maltoni and T. Stelzer, J. High Energy Phys. **0302**, 027 (2003) [arXiv:hep-ph/0208156].
- [29] J. Pumplin, D. R. Stump, J. Huston, H. L. Lai, P. Nadolsky and W. K. Tung, JHEP **0207**, 012 (2002) [arXiv:hep-ph/0201195].
- [30] J. Alwall, M. Herquet, F. Maltoni, O. Mattelaer, T. Stelzer, JHEP **1106** (2011) 128.
[arXiv:1106.0522 [hep-ph]].